High- and Low-Angle Normal Fault Activity in a Collisional Orogen: The Northeastern Granada Basin (Betic Cordillera)

Asier Madarieta-Txurruka[1] , Jesús Galindo-Zaldívar[1,2] , Lourdes González-Castillo[1] , José A. Peláez[3] , Antonio M. Ruiz-Armenteros[4,5] , Jesús Henares[6] , María Selmira Garrido-Carretero[4,5] , Manuel Avilés[4] , and Antonio J. Gil[4,5]

[1]Departamento de Geodinámica, Universidad de Granada, Granada, Spain, [2]Instituto Andaluz de Ciencias de la Tierra (CSIC-UGR), Granada, Spain, [3]Departamento de Física, Universidad de Jaén, Jaén, Spain, [4]Departamento de Ingeniería Cartográfica, Geodésica y Fotogrametría, Universidad de Jaén, Jaén, Spain, [5]Centro de Estudios Avanzados en Ciencias de la Tierra, Energía y Medio Ambiente (CEACTEMA), Universidad de Jaén, Jaén, Spain, [6]Universidad Internacional de La Rioja, Logroño, Spain

Abstract Understanding active tectonics and seismicity in extensional settings requires the analysis of high-angle normal faults (HANFs) and the transfer of deformation at depth. The debate surrounds the role of low-angle normal faults (LANFs) in triggering high magnitude earthquakes. The central Betic Cordillera is an active seismic zone affected by the NNW-SSE Eurasia-Nubia convergence and orthogonal extension. The seismicity and present-day stress determined by earthquake focal mechanisms reveals the activity of a NE-SW extensional system in the shallowest 12 km of the Granada Basin. The structure of the sedimentary infill, as derived by geological field and gravimetric techniques, suggests the formation of a half-graben tilted to the N-NE. Seismologic data suggest the activity of HANFs above 6–7 km depth and a LANF zone around 6–12 km depth, with related earthquakes of up to Mw 4.0 and 20° to 30° fault dips. High-precision leveling lines highlight the importance of the Granada Fault in the system, with average vertical displacement rates of 0.35–1.1 mm/yr. These data suggest creep fault behavior at the surface and increased seismicity at depth. The upper crustal extension in the collisional Betic Cordillera is accommodated by a top-to-the-WSW extensional detachment related to westward motion and rollback in the Gibraltar Arc and the gravitational collapse of the cordillera, in a framework of NNW-SSE shortening. This comprehensive study draws a new scenario that advances understanding of relationships between HANFs and LANFs.

1. Introduction

Low-angle normal faults (LANFs) or extensional detachments have been mapped and analyzed in numerous areas under extension (Abers, 1991; see review by Collettini, 2011) since they were first described in the Basin and Range province (Wernicke, 1981), although they also occur in compressional settings (Searle & Lamont, 2020). Geological studies suggest they are fundamental structures during the accommodation of crustal extension, often related to the omission of several tens of kilometer of stratigraphic thickness and generally linked to the exhumation of metamorphic core complexes (Grobe et al., 2019; Rey et al., 2011; Rosenberg & García, 2011). Despite their geological relevance (Hayman et al., 2003; Jolivet et al., 2010), the activity of LANFs in the upper crust and their relationships with large earthquakes are still under debate. Shedding light on this issue, Floyd et al. (2001) proposed that LANFs could become active due to hydrothermal fluid flow and high extensional stresses. According to a Coulomb's criterion (Anderson, 1951), normal faults initiate close to the Earth's surface, with dip angles in the range of 58°–68° (Sibson, 1985). Statistical studies of earthquakes (Collettini & Sibson, 2001; Jackson & White, 1989) show that earthquakes of $M > 5.5$ are restricted to a fault dip range of around 30°–60°, while no major earthquakes are observed with fault plane solutions having dips gentler than 20°. In this context, some authors concluded that LANFs could in fact be high-angle faults that were subsequently rotated (Proffett, 1977; Wernicke & Axen, 1988). Numerous microseismic studies of the Gulf of Corinth (Rigo et al., 1996), the Alto Tiberina Fault (Chiaraluce et al., 2007), the Brenner Fault (Reiter et al., 2005), and the Zucalle Fault (Piccinini et al., 2003) pointed to LANFs as structures that produce low-magnitude seismicity. The highest extension rates of

known LANFs evidenced by high-precision geodetic measurements (e.g., Basin and Range province; Niemi et al., 2004) do not agree with the small seismicity of LANFs (Abers et al., 1997). Further research (Collettini & Holdsworth, 2004; Hreinsdóttir & Bennett, 2009; among others) put forth that a major part of deformation is produced aseismically, an interpretation that was later demonstrated through detailed geodetic (e.g., Anderlini et al., 2016) and microseismicity studies (e.g., Gualandi et al., 2017), carried out in the Alto Tiberina Fault. In turn, in the Woodlark Basin, two recorded events of Mw 6.7 and 6.3 had respective focal mechanisms with nodal planes of 24° and 32° dip (Abers et al., 1997). Recently, Biemiller et al. (2020) described the possible occurrence of Mw > 7.0 earthquakes related to LANFs during the Holocene in this basin. Extensional detachment systems are usually accompanied by high-angle normal faults (HANFs) that affect the hangingwall of LANFs (Wernicke, 1981). HANFs tend to be related to higher seismicity and may be responsible for earthquakes of greater magnitude, either synthetic (Corinth Gulf; Rigo et al., 1996) or antithetic (Alto Tiberina Fault; Boncio et al., 2004; Chiaraluce et al., 2004). To contribute to our understanding of LANFs and their relationship with HANFs, it is necessary to carry out detailed studies of the active LANFs of different extensional settings.

The central Betic Cordillera (Figure 1) is a key region to study normal fault development in a collisional orogen. During the lower and middle Miocene, active LANFs exhumed the metamorphic complexes of the Internal Zones (Galindo-Zaldívar et al., 1989; Jabaloy et al., 1993). This is the case of the Mecina detachment, outcropping in Sierra Nevada and Sierra de los Filabres antiforms (Figure 1), considered to be active in that sector from Burdigalian to Early Tortonian times (Jabaloy et al., 1992; Vissers et al., 1995). The detachment was later exhumed due to the development of E-W folds in the framework of Eurasian and African convergence (García-Dueñas et al., 1986; Martínez-Martínez et al., 2002), and may have remained active only in the westernmost Sierra Nevada (Galindo-Zaldívar et al., 1996, 1999). At present, the most relevant set of active extensional faults are high angle, with NW-SE orientation, and located mainly in Neogene-Quaternary basins (Galindo-Zaldívar et al., 2003; Figure 1). To the north, the Baza Fault dips northeastward (Alfaro et al., 2008; Medina-Cascales et al., 2020). However, in the southern part of the Cordillera, most faults dip to the SW, including the Almeria-Tabernas (Marín-Lechado et al., 2005; Sanz de Galdeano et al., 2010), Balanegra (Galindo-Zaldívar et al., 2013; Marín-Lechado et al., 2010), and Padul fault zones (Gil et al., 2017), the latter extending toward the Granada Basin (Granada Fault zone; Morales et al., 1990; Rodríguez-Fernández & Sanz de Galdeano, 2006; Ruano et al., 2004). These HANFs affect the basement, but do not cut through the Mecina detachment (Galindo-Zaldívar et al., 1996).

The Granada Basin is of great interest because it is located next to Sierra Nevada, the region with the highest elevation (Sanz de Galdeano & Alfaro, 2004) and uplift rates (Braga et al., 2003) of the cordillera (Figure 1). It is the largest extensional basin of the Betic Cordillera and shows the greatest changes in GPS displacement rates (Galindo-Zaldívar et al., 2015; Garate et al., 2015). This area of high seismicity harbors the January 2021 earthquake swarm and subsequent activity (SIS, 2021). Aside from its present-day fault activity in a complex structural setting, where focal mechanisms of earthquakes related to NE-SW extension are the most frequent, and the basin features other strike-slip and even reverse focal mechanisms (Galindo-Zaldívar et al., 1999; Morales et al., 1997). One relevant population of earthquake focal mechanism is represented by events with low dip of one of the nodal planes. The main event of this population is the October 9, 2018 (Mw 4.0) earthquake in the central part of the Granada Basin (Figure 2). These focal mechanisms raise questions about the present-day activity of deep LANFs linked to shallow HANFs, or alternatively the occurrence of deep HANFs with vertical slips. To elucidate this issue, a comprehensive analysis of this fault system in the area is needed.

In this contribution, we aimed to recognize the main features of the active fault system of the Granada Basin with medium-high exposure risk given its location close to the metropolitan area of Granada, combining geological fieldwork, seismological, and gravity studies, and two high-precision leveling lines in the Granada Fault. With the multidisciplinary approach we developed in the Granada Basin, we strived to document the presence and role of buried active normal faults and their relevance for the seismic potential and hazard assessment.
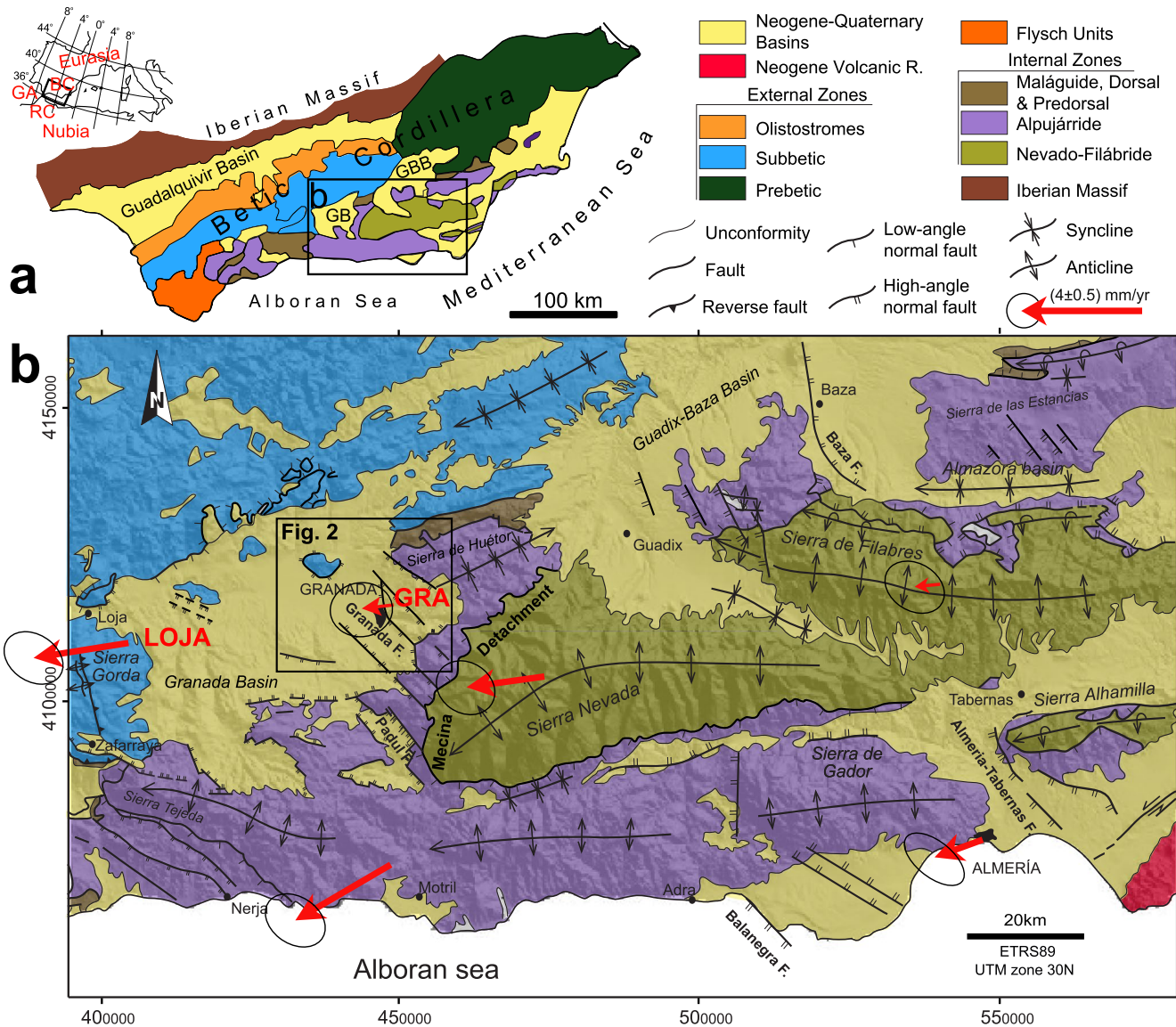
Figure 1. Geological setting of the central Betic Cordillera. (a) Synthetic sketch of the study area in the Betic Cordillera. BC, Betic Cordillera. GA, Gibraltar Arc. RC, Rif Cordillera. GB, Granada Basin; GBB, Guadix-Baza Basin. (b) Tectonic map with the location of main normal fault zones, modified from Galindo-Zaldívar et al. (2003). Note the location of the outcropping Mecina detachment. CGPS velocities from Galindo-Zaldívar et al. (2015) are shown with red arrows.

2. Geological and Seismological Setting

The Betic Cordillera (Figure 1), together with the Rif, constitute the westernmost alpine mountain belt in the Mediterranean area. The two mountain ranges are connected by the Gibraltar Arc and they surround the Alboran Sea. The Betic Cordillera is formed by the so-called Internal (Alboran Domain) and External (South Iberian Domain) Zones, separated by the Flysch Units. The Internal Zones are made up of three main tectonically superimposed complexes (from bottom to top: Nevado-Filábride, Alpujárride, and Maláguide), mostly metamorphized, in addition to the Dorsal and Predorsal complexes (Sanz de Galdeano et al., 2001). The External Zones constitute the fold-and-thrust belt of Mesozoic-Cenozoic rocks, generally located over Triassic rocks (Pérez-López & Sanz de Galdeano, 1994). Neogene-Quaternary basins are located above the Internal and External Zones (Sanz de Galdeano, 1990).

The main deformation in the Betic Cordillera started in the Cretaceous, implying shortening and major dextral displacement between the External and Internal Zones until the Oligocene (Sanz de Galdeano, 1990).
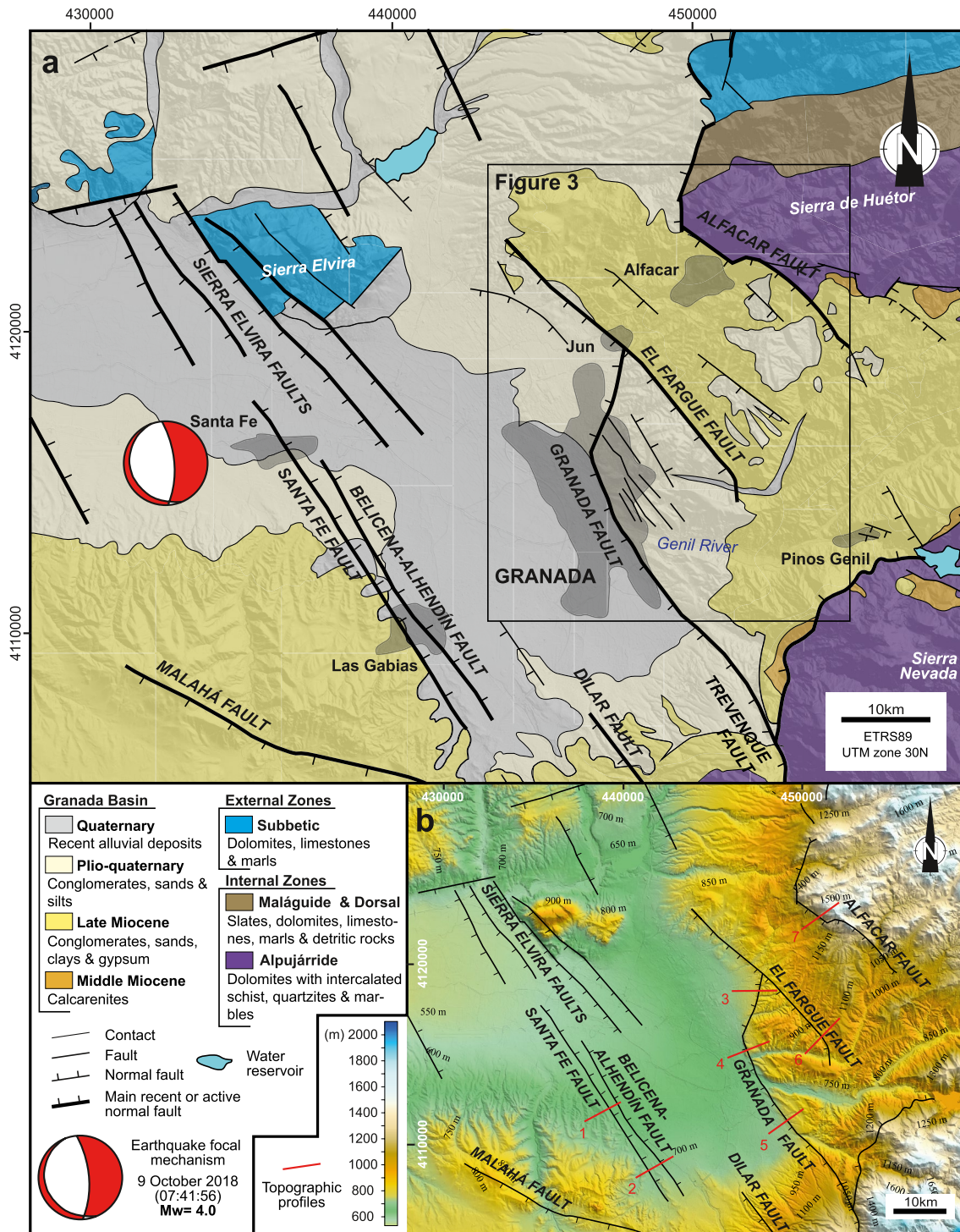
Figure 2. (a) Geological setting of the eastern Granada Basin with the main recent and active faults, including the location of the Mw 4.0 earthquake, on October 9, 2018, near Santa Fe. Modified from Galindo-Zaldívar et al. (2015). The location of this area is indicated in Figure 1. (b) Topographic map of the eastern Granada Basin with the main recent and active faults. Locations of the topographic profiles of Figure 4d.

This main contact became inactive in, at least, the middle Miocene, after which N-S to NNW-SSE compression with perpendicular extension (Braga et al., 2003; Sanz de Galdeano & Alfaro, 2004) affected the Betic Cordillera. The Internal Zones underwent intense ENE-WSW extension, producing crustal thinning, the exhumation of the metamorphic complexes, and the development of LANFs (e.g., Mecina detachment;

Galindo-Zaldívar et al., 1989; Jabaloy et al., 1992). Since the Tortonian, the Eurasian-Nubian plate convergence and orthogonal extension have continued, producing E-W oriented dextral and normal faults, conjugate NW-SE dextral faults, and NE-SW sinistral and normal faults together with large E-W and NE-SW folds (Galindo-Zaldívar et al., 2003; Sanz de Galdeano, 1990). The Neogene-Quaternary Guadalquivir foreland basin developed at the front of the Cordillera together with the large Alboran Sea in its southeastern part and smaller intramontane basins, such as the Granada and Guadix-Baza basins.

Different models have been proposed for the development of the Betic-Rif Cordillera and to explain the causes of extension in the central zone. Subduction models (Araña & Vegas, 1974; Chertova et al., 2014; de Jong, 1991, 1993; Morales et al., 1999; Thiebot & Gutscher, 2006; Torres-Roldán et al., 1986; Wortel & Spakman, 1992), some of them including slab rollback (Brun & Faccenna, 2008; Gill et al., 2004; González-Castillo et al., 2015; Hoernle et al., 1999; Lonergan & White, 1997; Morley, 1993; Pedrera et al., 2011; Pérouse et al., 2010; Ruiz-Constán et al., 2011), delamination models (Calvert et al., 2000; García-Dueñas et al., 1992; Houseman et al., 1981; Mancilla et al., 2013; Platt & Vissers, 1989; Seber et al., 1996), and slab tearing or detachment models (Blanco & Spakman, 1993; Spakman et al., 2018; Zeck, 1996; Zeck et al., 1992) have been discussed. Some authors combine the former models, considering slab detachment with rollback (Wortel & Spakman, 2000), delamination with rollback (Fadil et al., 2006), or delamination with slab tearing (Mancilla et al., 2015).

The current development of the Betic Cordillera is a consequence of oblique dextral convergence of 4.0 ± 0.2 mm/yr between the Eurasian and Nubian plates in a NNW-SSE direction (DeMets et al., 2010; Iribarren et al., 2007) and coeval westward motion with respect to the surrounding plates (Galindo-Zaldívar et al., 2015; Garate et al., 2015; Koulali et al., 2011). Simultaneous with cordillera uplift (Braga et al., 2003; Reinhardt et al., 2007), the shallow crust has been deformed by NW-SE fault zones (Baza, Tabernas-Almeria, Balanegra, Padul, and Granada faults), connected by dextral and transtensional transfer faults (Galindo-Zaldívar et al., 2015).

Seismicity due to the Eurasian-Nubian plate boundary convergence is heterogeneous and widespread in the cordillera (Buforn et al., 2004; Morales et al., 1997). Although shallow activity predominates, some intermediate seismicity also occurs (up to 150 km depth) in the western Alboran Sea (Santos-Bueno et al., 2019), in addition to deep seismicity (650 km depth; Buforn et al., 2011) to the south of Granada. Given the heterogeneous distribution of seismicity in the Betic Cordillera, it is not always possible to correlate it with the outcropping faults (Galindo-Zaldívar et al., 1999).

The intermontane Granada Basin (Figures 1 and 2) is an extensional basin located on the boundary between the External and Internal Zones of the Betic Cordillera, filled with middle Miocene to Pliocene-Quaternary sediments. The basement of the Granada Basin is formed by metamorphic rocks of the Internal Zones (in its southeastern half) and sedimentary rocks of the External Zones (in its northwestern half). Lying unconformably on the basement, the sedimentary infill contains marine sediments of Serravallian and late Tortonian age (Fernández & Rodríguez-Fernández, 1991). Above, the thick evaporitic deposits (gypsum and salt) in the southern part of the basin are related to the final retreat of the sea in the latest Tortonian-Messinian (Rodríguez-Fernández & Sanz de Galdeano, 2006). In the northeastern part, clastic sediments are predominant, deposited by large alluvial fans. In late Mesinnian time, the western part was partially occupied by lakes, as documented by lacustrine limestones. During the Pliocene, fluvial conglomerates, sands and clays, and lacustrine limestones were deposited. Finally, in the Pleistocene, the basin was captured by the Guadalquivir River drainage system, developing the current alluvial plain. The eastern border was drained by alluvial fan systems (Rodríguez-Fernández & Sanz de Galdeano, 2006; Ruiz-Bustos, 2002) including the conglomeratic Alhambra Formation, which was formed by the erosion and subsequent deposition of rocks eroded from Sierra Nevada.

The Granada Basin is bounded by a set of E-W, ENE-WSW to NE-SW strike-slip and normal faults, at the northern and southern boundaries. The northeastern region (Figure 2) is affected by NW-SE normal faults (Morales et al., 1990; Rodríguez-Fernández & Sanz de Galdeano, 2006; Ruano et al., 2004). The faults located to the NE (Alfacar, El Fargue, Granada, and other smaller ones) dip toward the SW and generate the largest topographic high and biggest associated scarps (Figure 2b). The faults located in the SW (Santa Fe and Belicena-Alhendín) dip toward the NE and the related topographic high is smaller. To the SW, the Malahá
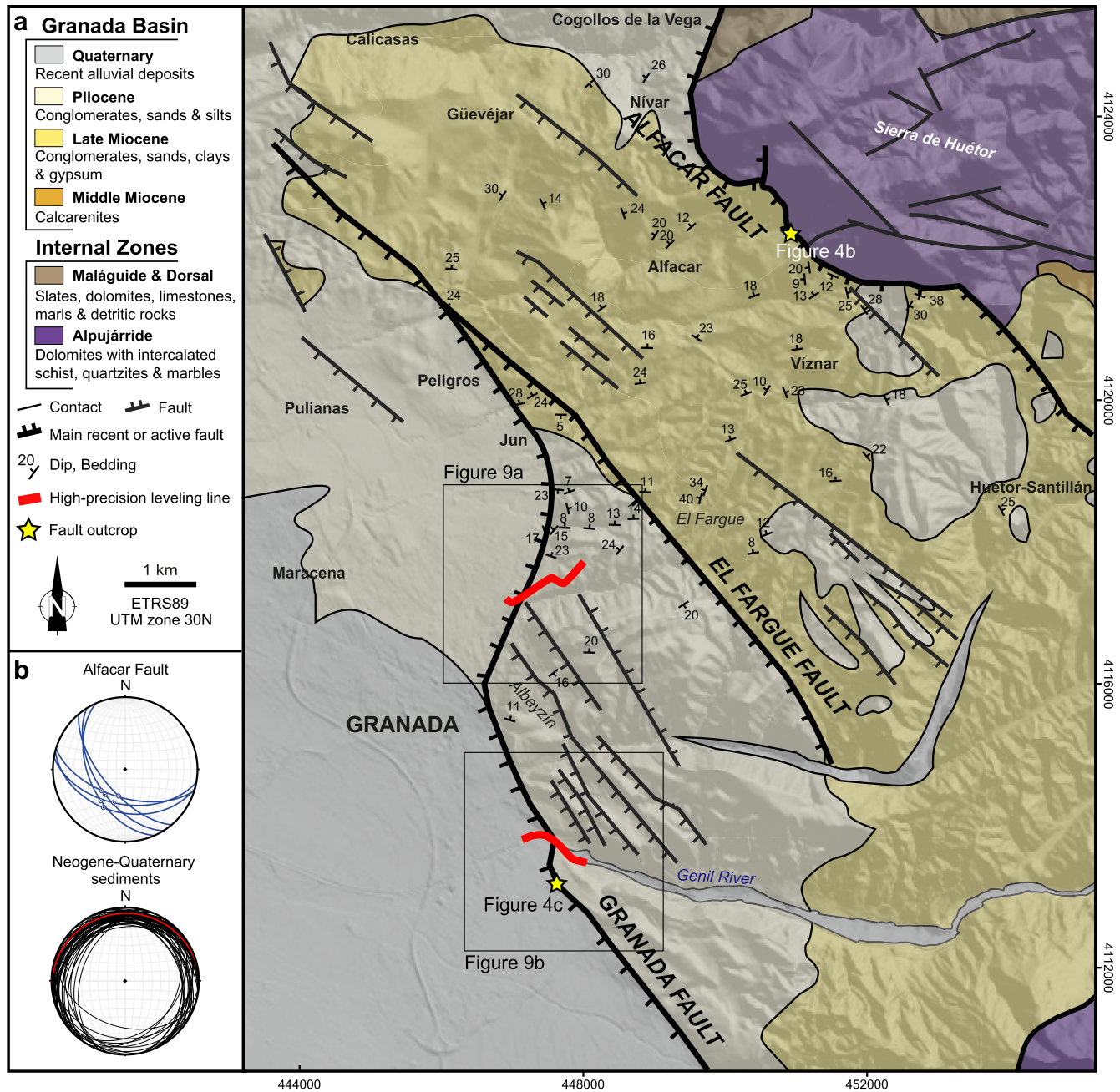
Figure 3. (a) Detailed geological map of the northeastern edge of the Granada Basin, including the main tectonic structures, modified from Galindo-Zaldívar et al. (2015). Location of outcrops illustrated in Figure 4 and high-precision leveling lines are indicated. The location of this area is given in Figure 2. (b) Stereonets (Schmidt net, lower hemisphere) of dip/dip directions of the Alfacar fault and the Neogene-Quaternary sediments.

Fault has a WNW-ESE orientation and dips to the SSW. In addition, there are more normal NW-SE faults dipping toward the SW next to Sierra Elvira and in the SE of the study area, near Sierra Nevada (García-Mayordomo et al., 2012; QAFI, 2021). Moreover, NE-SW and E-W fault sets occur in the region (Figures 2 and 3). These fault sets develop half-graben structures with sediment tilting toward the NNW (Rodríguez-Fernández & Sanz de Galdeano, 2006; Ruano et al., 2004; Figure 3b). The activity of these faults is supported by paleoseismic research (Azañón et al., 2013; Sanz de Galdeano et al., 2003, 2012), as well as the geomorphic (Carvajal & Sanz de Galdeano, 2001; Pérez-Peña, 2015; Pérez-Peña, Azañón, Azor, et al., 2009; Pérez-Peña, Azañón, Booth-Rea, et al., 2009), geological (Galindo-Zaldívar et al., 1999), and seismological data (Morales et al., 1997).

3. Methodology

3.1. Study of the Tectonic Structures

Fieldwork was undertaken (Figures 3 and 4) with the aim of determining the major structures in the area and to study their fault outcrops, scarps, and related deposits. A regional reconnaissance of lithology and bedding was carried out to characterize the features of the main folds and faults. Fault scarps and surfaces were observed in detail to establish their recent activity. The main structural features—including fault surface orientation and dip, grooves, and striae orientations—provide information on the fault kinematics. Moreover, iron mineralizations on fault surfaces were observed (Figure 4b).

Fault scarps are the primary geomorphic expression of active faulting at surface (Stewart & Hancock, 1991). Faults with slip rates higher than 0.3–0.4 mm/yr tend to generate postglacial scarps in the Mediterranean (e.g., Benedetti et al., 2002; Cowie et al., 2017; Tucker et al., 2011). For their study, in addition to field observations, topographic profiles perpendicular to the faults were obtained (Figure 4d) using the 5 m pixel accuracy DTM developed by the Spanish Instituto Geográfico Nacional (IGN) (CNIG, 2021).

3.2. New Gravity Data and Models

Gravity research constitutes a reliable technique for determining the basement relief and the sedimentary infill geometry given the contrast between the relatively low density of the sedimentary infill and the high density of the basement. In the studied sector of the Granada Basin, 203 new gravity measurements were acquired, distributed in four profiles perpendicular to the main faults of the northeastern basin (Figure 5). The locations were determined using a Leica Zeno 20 differential GPS, with accuracy higher than 1 m. The gravity measurements were performed using a Scintrex Autograv CG-5 relative value gravimeter, which provides a standard accuracy of 0.001 mGal, and were referred to the gravity base of the Spanish IGN in Granada (Absolute gravity, 2021). The Bouguer anomaly was computed using a density value of 2.67 g/cm^3, while the topographic correction was computed using a 5 m pixel resolution DTM developed by the IGN (CNIG, 2021) up to a distance of 80 km from the stations, combining Kane's (1962) and Nagy's (1966) methods. A new Bouguer anomaly map was calculated based on the 203 new gravity measurements and the 657 older ones compiled during the project TopoIberia in the same region (Ayala et al., 2016; SIGEOF, 2021; Figure 5a). The regional anomaly was obtained by means of first-order polynomial fitting, as proposed by Martínez-Moreno et al. (2015; Figure 5b). The residual anomaly was obtained by subtracting the regional anomaly from the Bouguer anomaly (Figure 5c). In addition, four residual gravity anomaly profiles were depicted, then modeled using the Gravmag 1.7 code of the British Geological Survey (Pedley et al., 1993; Figure 6). The estimated density values are 2.67 g/cm^3 for the basement (Hinze, 2003) and 2.3–2.5 g/cm^3 for the sedimentary infill, according to the average values of the dominant lithologies (Telford et al., 1990).

3.3. Seismicity

The study of seismicity involves temporal and spatial analysis to shed light on the current activity of faults at depth. In addition, study of the focal mechanisms is used to associate earthquakes with surrounding faults. For these reasons, the seismicity of the study area—available from the IGN database—was combined and plotted (Figure 7a; SIS, 2021). Events after 2000 were exclusively taken into account, due to their higher accuracy even for low-magnitude events (location error < 1–2 km; González, 2017); only shallow seismicity (less than 15 km depth, below which seismicity decreases) is considered to bear relation with the extensional system. In addition, the brittle-ductile transition is estimated to be around 17–18 km deep, based on P- and S-wave tomography (Serrano et al., 2002) and previous seismicity analysis in the basin (Galindo-Zaldívar et al., 1999; Morales et al., 1997). Focal mechanisms at depths shallower than 15 km including the older data (since 1985) were compiled from previous research and the IGN database (SMT, 2021) (Figure 7b; Table 1), and the stress tensor was calculated from them (Figure 7d). To analyze the distribution of seismicity with depth, we considered general seismic patterns, given the error in depth location. For this purpose, we constructed an earthquake density grid with the events that have assigned depth (Figure 7c), projecting the earthquakes on a profile parallel to the extension. The January 2021 swarm data were not introduced in the grid; because it comprises more than half of the events since 2000 (see histogram in Figure 7a) yet is associated with a single structure and blurs the distribution.

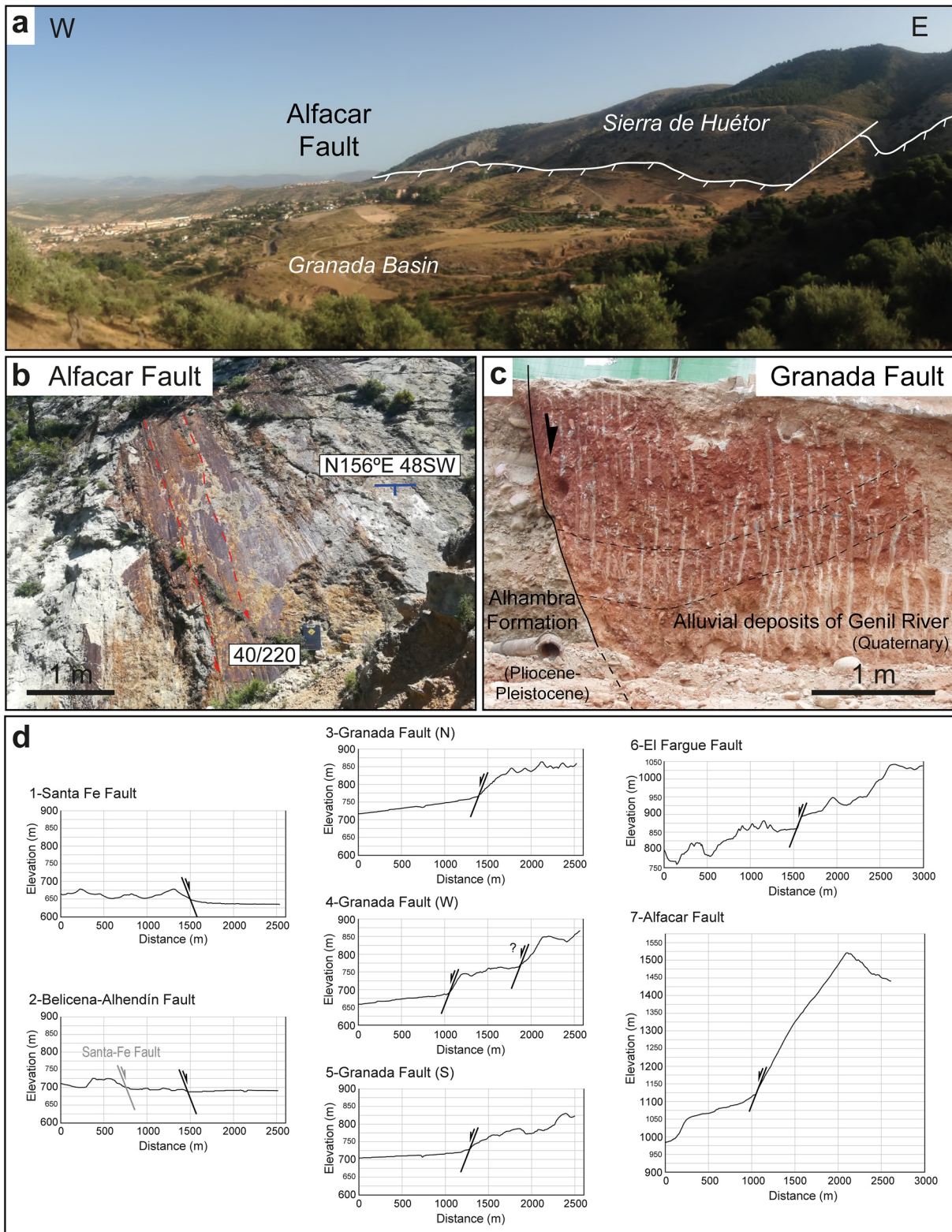**Figure 4.** Main faults in northeastern Granada Basin. (a) The Alfacar Fault in the mountain front of the Sierra de Huétor. (b) Outcrop of the Alfacar Fault surface, where iron mineralizations with striae mark the fault surface. (c) The Granada Fault to the south of Granada, next to the Genil River. Locations in Figure 3. (d) Topographic profiles perpendicular to the faults, Vertical Exaggeration = 5. Locations in Figure 2b.
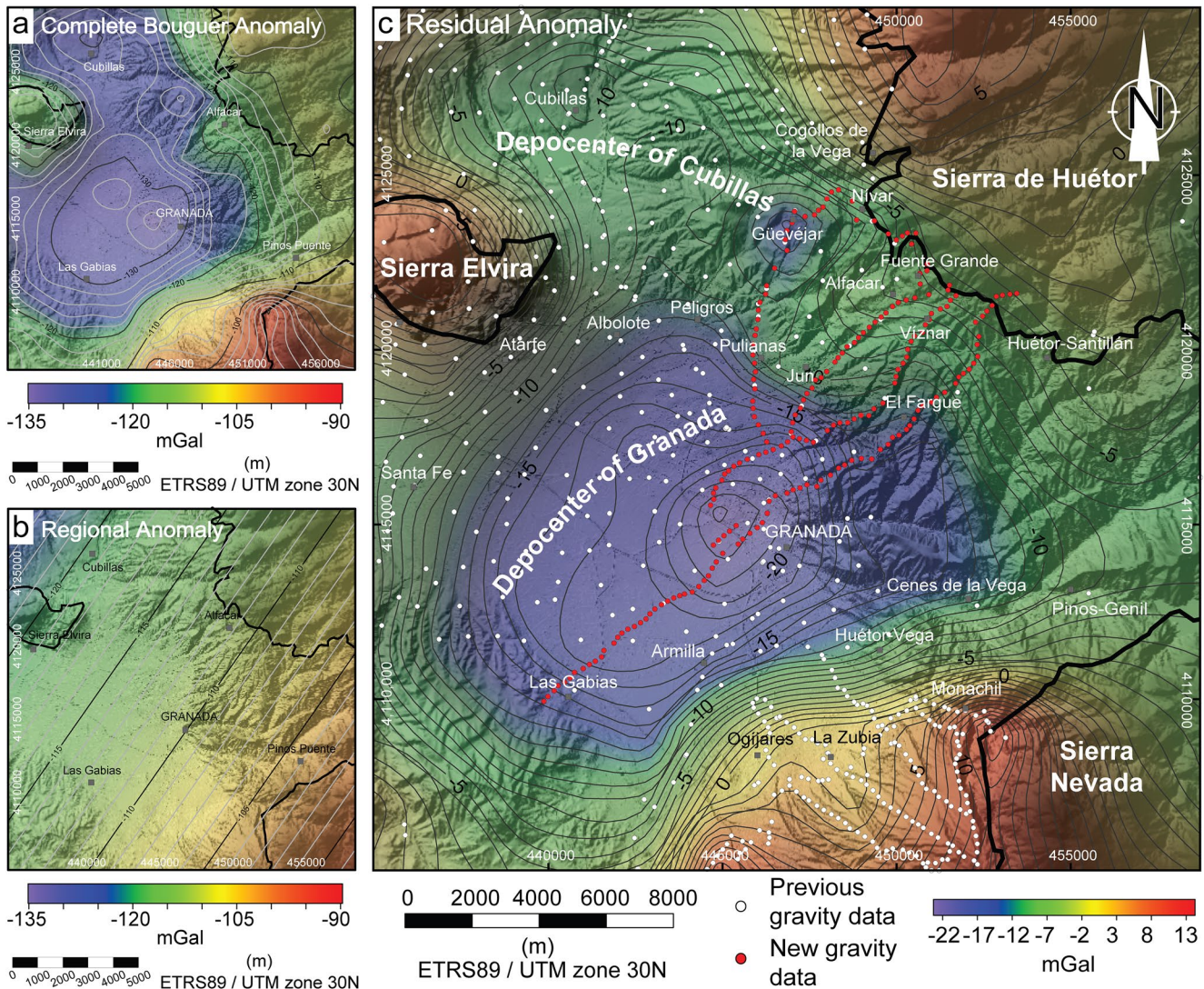
Figure 5. Gravity anomaly maps. The boundary of the basin is marked with a black line. (a) Complete Bouguer anomaly map, (b) regional anomaly map, and (c) residual anomaly map with the gravity station positions.

3.4. High-Precision Leveling

High-precision leveling data collected over several years can be used to quantify vertical movements with high precision and thus monitor active normal faults, including identifying seismic and creep deformation (Galindo-Zaldívar et al., 2013; Giménez et al., 2009; Marín-Lechado et al., 2010). The fault slip rates obtained can in turn be compared with long-term geological or geomorphological slip rates.

Two high-precision leveling lines crossing the Granada Fault were established by Ruiz et al. (2003). When installing a high-precision leveling line, several factors that generate vertical displacements in the terrain must be taken into account. First, the tectonic influence must be quantified. Second, lithology, landslides, and settlements must be considered. Finally, a change in the water table can generate subsidence or uplift. To minimize such noise, the locations for benchmarks were installed with the following considerations: (a) slopes are low (Figure 8); (b) in urbanized areas, constructions are old enough to have already settled; (c) there are no nearby water extraction wells. One of these lines consists of 16 benchmarks (J#), along the local Granada-Víznar road in Jun (Figures 3 and 8a). The second one includes 14 benchmarks (G#) and runs along a wall on the pavement in southern Granada, parallel to the Genil River (Figures 3 and 8b).
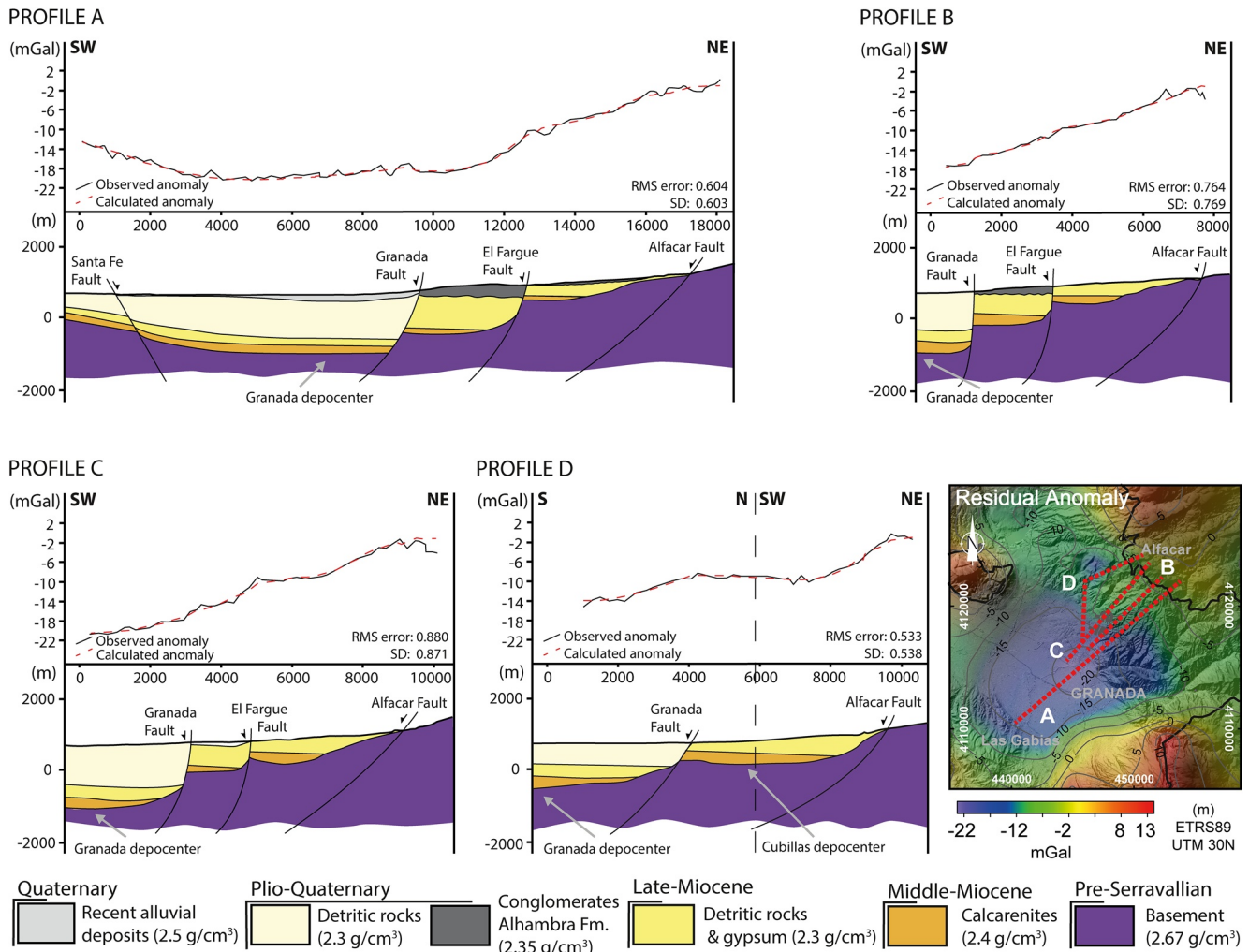
Figure 6. Gravity residual anomaly profiles (top) and gravity associated models (bottom). Location of the profiles in the residual anomaly map.

Both leveling lines were surveyed from 1999 to 2013 by the Microgeodesy Research Group of the University of Jaén (Spain), using precision levels and invar rods. A Wild N3 optical level with a parallel plate micrometer was used for the 1999 survey, and a Wild NA3003 digital level for the 2000 survey. Early results were published by Ruiz et al. (2003). Since 2000, three new surveys have been carried out with a Leica DNA03 digital level: (a) in September 2009 for both lines, and (b) in September 2011 and February 2013, only for the Genil line, because most of the benchmarks along the Granada-Viznar road had been destroyed. For every benchmark, we evaluated the difference between the height in each survey and the height in the first one (1999), together with the propagated expanded uncertainty for such differences (Figure 8).

4. The Structure of NE Granada Basin and the Main Extensional Faults

4.1. Field Tectonic Features of the Main Faults

The northeastern boundary of the Granada Basin is characterized by NW-SE oriented normal faults (Figures 2–4). The main faults that affect the Internal Zones are the 5.3-km long Alfacar Fault, the 11.6-km long El Fargue Fault, and the 16.8-km long Granada Fault (Sanz de Galdeano et al., 2003, 2012). Moreover, smaller normal faults can be found in the area associated with the main ones (Azañón et al., 2004; Lupiani & Soria, 1988). The southwestern boundary is also deformed by the Belicena-Alhendín, Santa Fe, and Malahá faults.
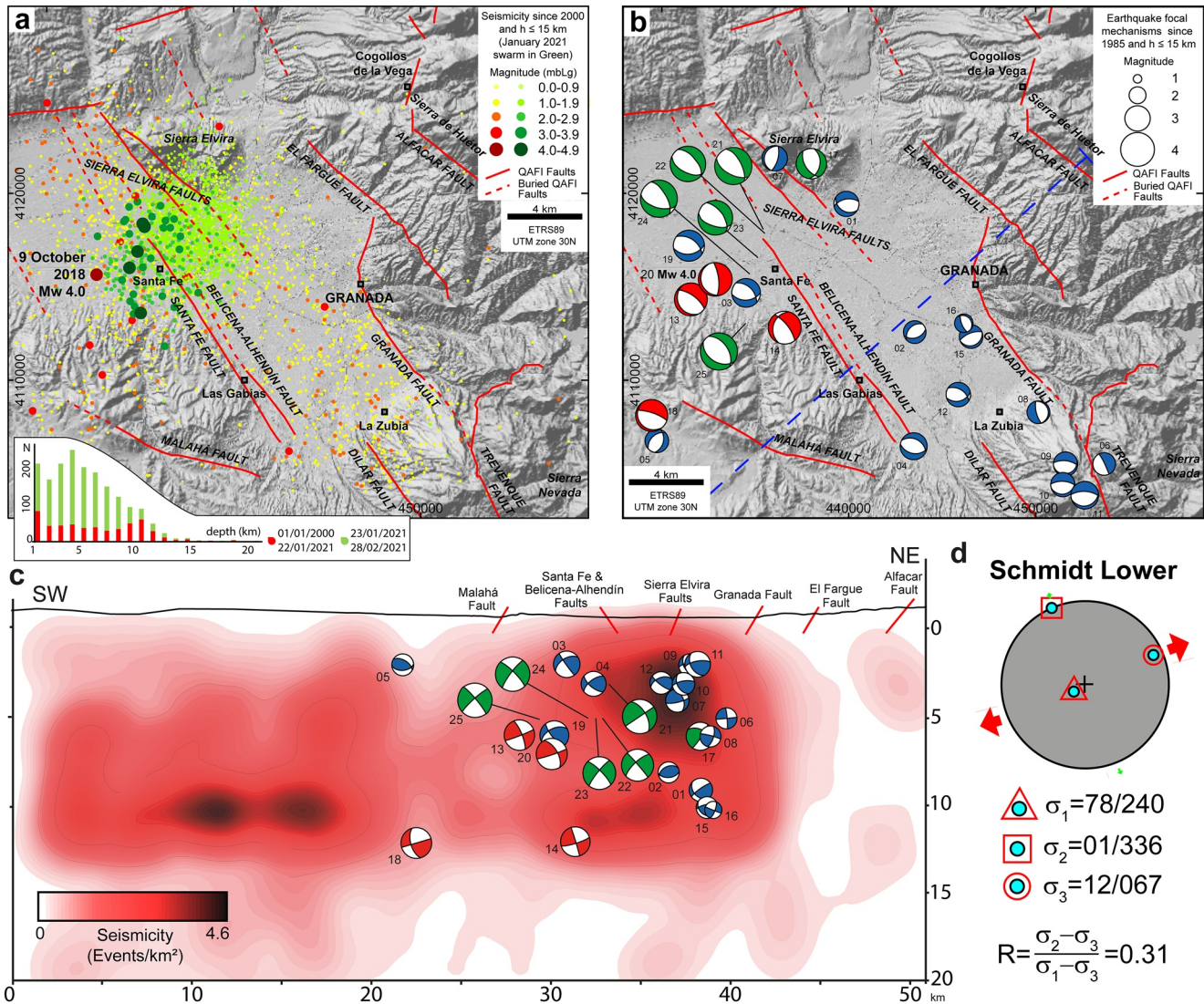
Figure 7. Seismicity in northeastern Granada Basin. (a) Seismicity since year 2000 that is shallower than 15 km depth from Instituto Geográfico Nacional database (SIS, 2021). Histogram of seismic distribution with respect to depth, background seismicity in red (January 1, 2000 to January 22, 2021) and January 2021 swarm in green (January 23, 2021 to February 28, 2021) (left-bottom). (b) Earthquake focal mechanisms since 1985 that are shallower than 15 km depth. Numbers correspond to Table 1 mechanism solutions. (c) Profile perpendicular to the main faults showing the available focal mechanisms including the January 2021 swarm, and the projection of the density grid of background seismicity (January 1, 2000 to January 22, 2021). (d) Reduced stress tensor: Orientation of the main stress components and the axial ratio are shown.

The Alfacar Fault (Figures 3 and 4) is located at the boundary between the Granada Basin and the Alpujárride Complex, which emerges in the Sierra de Huétor. The fault has an average strike of N129°E and an average dip of 50°SW, but locally exhibits an undulating surface (Figure 3b). The fault surface is characterized by the presence of striated iron mineralization and fault steps supporting a normal slip (Figure 4b). The related scarp reaches 450 m in height in the dolomites of the Alpujárride Complex (Figure 4d). The El Fargue Fault (Figure 3a), striking N138°E and with a maximum dip of 60°SW, cuts Plio-Quaternary conglomerates. A small scarp developed in Pleistocene rocks (Sanz de Galdeano et al., 2003, 2012) reaches 25 m in height (Figure 4d).

The Granada Fault (Figure 3a), striking N150°E, crosses the city of Granada, and dips 60°SW. To the north, it bends and strikes N-S. The associated scarp can only be observed to the north (Figures 4d, 7b and 9a) and south of the city (Sanz de Galdeano et al., 2003, 2012) (Figures 4d and 9b), reaching up to 100 m in height. Several splays in the central sector affect late Pliocene-Pleistocene sediments of the Alhambra Formation

Table 1
Solutions for Shallow Earthquake Focal Mechanisms Represented in Figure 7b

N.	Date	Time (hh:mm:ss)	Long. (°E)	Lat. (°N)	Depth (km)	δh (km)	Magnitude	Strike (°)	Dip (°)	Rake (°)	RMS/CLVD
01[a,b]	April 7, 1985	14:01:03	−3.6800	37.2217	9	[c]	MbLg 3.0	259	62	−114	--
02[a,b]	May 24, 1985	19:04:51	−3.6383	37.1600	8	[c]	MbLg 2.7	225	45	−111	--
03[d]	August 20, 1988	16:42:52	−3.7400	37.1783	2	1.0	MbLg 3.4	85	48	−128	*0.4*
04[e]	October 7, 1989	04:45:11	−3.6383	37.1050	3	[c]	MbLg 3.2	101	45	−101	*0.12*
05[e]	July 1, 1990	23:24:05	−3.7933	37.1067	2	[c]	MbLg 2.8	15	45	−114	*0.17*
06[e]	June 21, 1991	21:24:01	−3.5233	37.0967	5	[c]	MbLg 2.7	334	85	−90	*0.17*
07[f]	August 8, 1991	03:31:58	−3.7233	37.2433	4	[c]	MbLg 3.0	15	70	−90	*0.12*
08[g]	February 7, 1992	16:29:15	−3.5633	37.1217	6	4.0	MbLg 2.7	165	75	−90	--
09[e]	March 21, 1993	08:17:38	−3.5467	37.0967	2	[c]	MbLg 2.9	76	23	−109	*0.24*
10[e]	March 21, 1993	09:55:26	−3.5483	37.0867	3	[c]	MbLg 2.9	76	23	−105	*0.21*
11[e]	March 21, 1993	10:01:40	−3.5350	37.0817	2	[c]	MbLg 3.3	76	23	−105	*0.24*
12[e]	December 6, 1994	09:28:55	−3.6117	37.1300	3	[c]	MbLg 2.9	75	45	−125	*0.15*
13[d]	March 17, 1995	14:04:14	−3.7733	37.1750	6	1.0	MbLg 3.9	305	70	−99	*0.6*
14[h]	December 28, 1996	07:30:37	−3.7167	37.1617	12	[c]	Mw 3.9	200	30	−36	0.15
15[g]	June 4, 1998	17:38:17	−3.6043	37.1580	10	4.0	MbLg 2.8	70	25	−90	--
16[g]	June 4, 1998	19:28:52	−3.6086	37.1645	10	4.0	MbLg 2.2	158	70	−79	--
17[g]	June 7, 1999	10:03:13	−3.7013	37.2409	6	4.0	MbLg 3.6	147	57	−118	--
18[i]	September 10, 2003	20:22:47	−3.7966	37.1189	12	2.0	Mw 3.8	289	76	−100	0.22
19[j]	January 4, 2007	23:32:32	−3.7747	37.2008	6	[c]	Mw 3.7	303	53	−62	0.01
20[k]	October 9, 2018	07:41:56	−3.7587	37.1848	7	0.1	Mw 4.0	354	73	−84	0.28
21[k]	January 23, 2021	11:15:24	−3.7239	37.2062	3	[c]	Mw 4.4	342	59	−75	0.09
22[k]	January 26, 2021	21:36:33	−3.7296	37.1951	5	[c]	Mw 4.1	318	49	−77	0.07
23[k]	January 26, 2021	21:44:18	−3.7330	37.1756	5	[c]	Mw 4.2	324	51	−67	0.16
24[k]	January 26, 2021	21:54:55	−3.7369	37.1843	5	[c]	Mw 4.4	329	53	−63	0.02
25[k]	January 28, 2021	18:49:49	−3.7206	37.1565	5	[c]	Mw 4.4	325	50	−75	0.02

Note. The last column displays the adjustment of the focal mechanism inversion indicated in RMS or CLVD.

Abbreviations: CLVD, compensated linear vector dipole; IGN, Instituto Geográfico Nacional; RMS, root mean square error.

[a]Vidal (1986). [b]Galindo-Zaldívar et al. (1993). [c]Not provided by the authors/institutions. [d]Herraiz et al. (1998). [e]Serrano (1999). [f]Serrano et al. (1996). [g]Martínez-Martínez et al. (2006). [h]Stich et al. (2003). [i]Stich et al. (2006). [j]Stich et al. (2010). [k]IGN (SMT, 2021).

(Azañón et al., 2004) (Figures 4d and 9b) that can be observed NE of the city or in outcrops near the Genil River (Figures 4c and 9b). The addition of the different scarps amounts to 175 m (Figure 4d).

Toward the SW (Figure 2), the Santa Fe and Belicena-Alhendin faults strike N146°E and dip 60°NE (Sanz de Galdeano et al., 2012). The Santa Fe Fault separates the Neogene and Quaternary deposits with a 30-m high-associated scarp (Figure 4d). The Belicena-Alhendín Fault crops out only to the south of the basin, affecting Quaternary sediments. It has an associated scarp of just 5–10 m. Toward the north, it becomes a blind fault, although it is still observable in seismic profiles (Sanz de Galdeano et al., 2012).

Northwestward and southeastward of the study area there are more faults pertaining to this set, dipping at about 60° SW (Figures 1 and 9). The faults bordering Sierra Elvira (QAFI, 2021) affect the External Zones. Toward the SE, the Trevenque Fault, the Dílar Fault, and the Padul-Nigüelas Fault zone (Gil et al., 2017) (Figures 2, 7 and 9b) limit the basin and continue through the Alpujarride Complex to join the Mecina detachment, but they do not deform the Nevado-Filabride Complex (Galindo-Zaldívar et al., 1996).

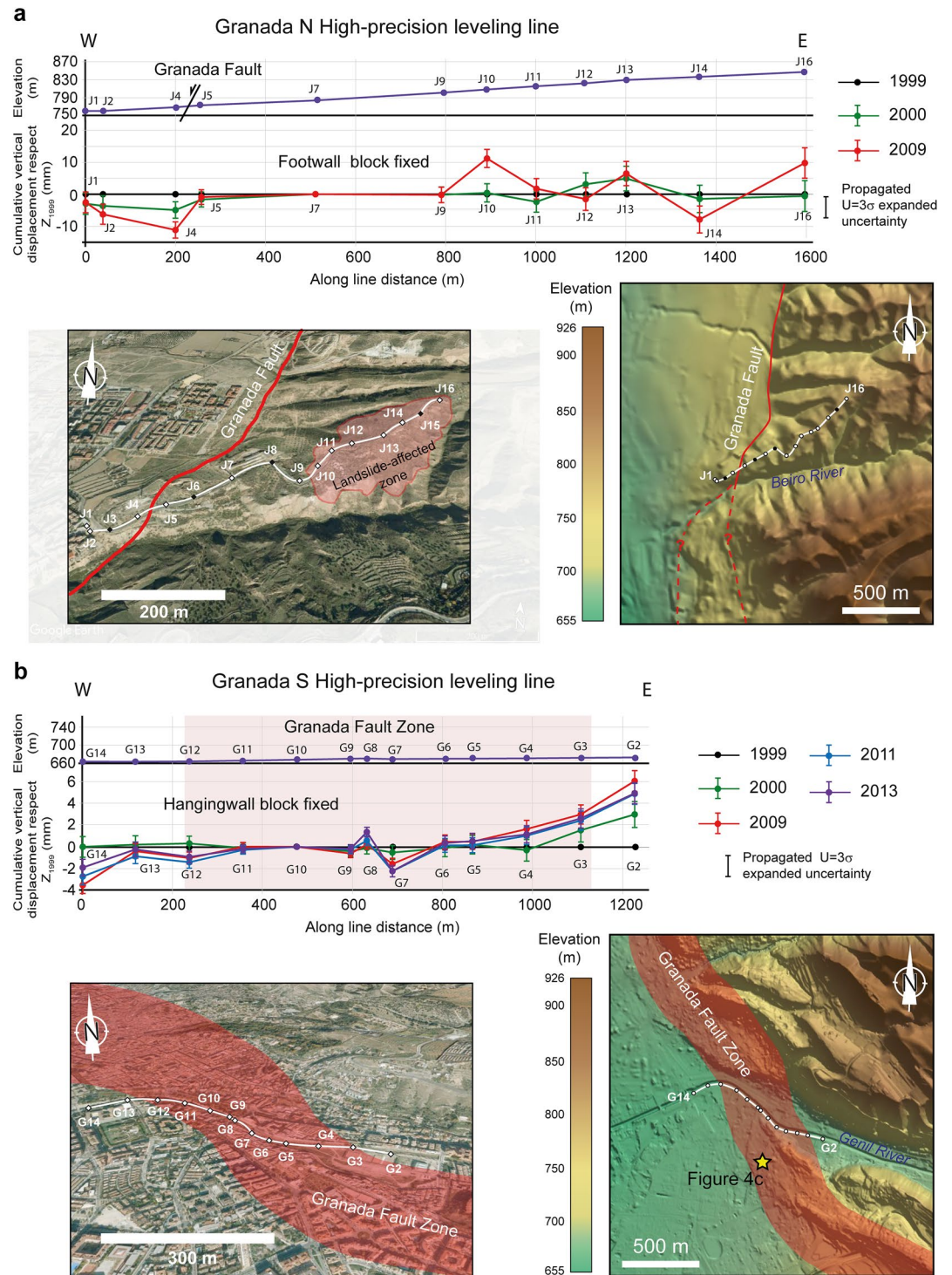**Figure 8.** High-precision leveling lines. (a) Granada N line: cumulative vertical displacements from 1999 to 2009, together with the propagated expanded uncertainty. (b) Granada S line: cumulative vertical displacements from 1999 to 2013 together with the propagated expanded uncertainty. Insets: Topographic profiles (top). High-precision leveling line in aerial view (lower left). Topographic map (lower right).
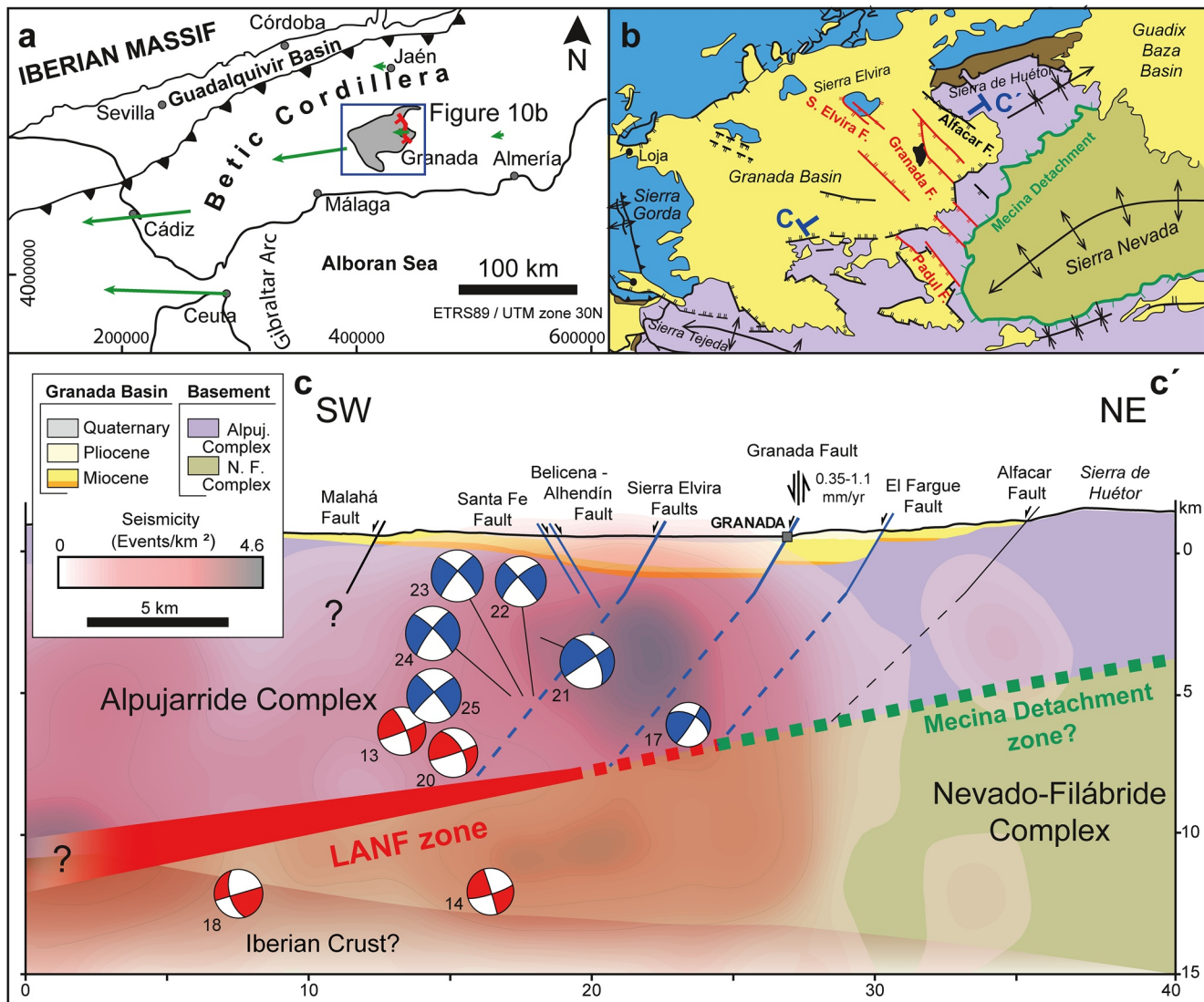
Figure 9. High-angle normal faults (HANFs) and low-angle normal faults (LANFs) system in the Granada Basin in the framework of the Betic Cordillera. (a) Location of Granada Basin in the Betic Cordillera, including some CGPS velocities (green arrows) from Galindo-Zaldívar et al. (2015) and González-Castillo et al. (2015). (b) Simplified geological map of Granada Basin, modified from Galindo-Zaldívar et al. (2003). (c) Cross section of HANF and LANF systems with the projection of rotated earthquake focal mechanisms (Mw > 3.5). Numbers correspond to Table 1 mechanism solutions: in red, those with a subhorizontal nodal plane. In blue, the focal mechanisms with nodal plane dips between 45° and 60°. The background seismicity density grid is also shown.

The deposits associated with the faults range in age from the middle Miocene, mainly on the NE edge of the basin, to the Quaternary, closer to Granada city. They have dips between 5° and 40°, generally with a northward component (Figure 3).

4.2. Gravity Data and Models

Gravity data reveal the structure of the basin at depth. The Bouguer anomaly map (Figure 5a) shows a range of values, between −134 and −92 mGal. Two gravity minima can be observed W of Granada and at the NW sector of the study area. However, the increase of the regional anomaly toward the SE (Figure 5b) should be removed to adequately determine the sedimentary infill geometry. The residual anomaly map (Figure 5c), ranging from −23 to 13 mGal, allows us to better identify the principal gravity minima associated with the Granada depocenter, around the city itself, and the Cubillas depocenter, north of the study area (Morales

et al., 1990; Rodríguez-Fernández & Sanz de Galdeano, 2006). The gravity maxima are related to the basement outcrops of Sierra Elvira, Sierra de Huétor, and south of Monachil.

The residual anomaly models of profiles A to D (Figure 6) reveal that the depocenter is located southwestward in model A, at 7 km from the beginning of the profile, and has an estimated 1,400–1,600 m maximum sedimentary infill (2.3–2.4 g/cm^3) above the basement (2.67 g/cm^3). The structure of the NE Granada Basin is marked by a northeastward staircase decrease of the sedimentary infill related to the Granada, El Fargue, and Alfacar faults. Yet in profile A, the gravity anomaly increases in the downthrown block due to the presence of Quaternary alluvial deposits formed mainly by debris boulders—therefore of higher density (2.5 g/cm^3; Telford et al., 1990)—next to the fault (Lupiani & Soria, 1988). Profile D again shows a decrease of the gravity value toward the SW and an increase of the slope at 4 km, due to the activity of the Granada Fault. At 8 km in this profile, however, another minor depocenter is observed, which would be related to the depocenter of Cubillas (Figure 5; Morales et al., 1990; Rodríguez-Fernández & Sanz de Galdeano, 2006).

5. Seismicity

The seismic record available since 2000 (Figure 7a) shows significant low-magnitude seismicity. There are only a few earthquakes over MbLg 3.0, and just six events over Mw 4.0 located around Santa Fe. One occurred on October 9, 2018 (#20 in Table 1), and the largest earthquakes correspond to the recent 2021 swarm (#21–25 in Table 1). From the spatial point of view, there is more seismicity SW of active fault traces than to the NE. Figure 7a differentiates the background seismicity (in reddish tones) from the January 2021 swarm (in greenish tones). The background seismicity has a fairly homogeneous distribution along a NW-SE band in the hangingwall of the Granada and Sierra Elvira faults. The 2021 swarm is located mainly NE of Santa Fe, in the hangingwall of the Sierra Elvira faults.

The available earthquake focal mechanisms are divided into main groups according to their location. Thirteen out of the 25 focal mechanisms are located northwestward, 10 southeastward, and the other two southwestward of the study area. In general, they present normal earthquake mechanism solutions in which the NW-SE nodal plane direction predominates. However, SE of the study area, E-W directions also are found. Twelve out of 20 of the focal mechanisms present one low-angle nodal plane. Numbers 13, 14, 18, and 20 stand out due to their higher magnitude (Mw > 3.5). The rest present nodal planes with dips between 45° and 60°. The focal mechanisms of the January 2021 swarm events have these characteristics.

Although the depth distribution of the data has lower accuracy than the epicentral location, some general observations can be made. The seismicity density grid (Figure 7c) shows: (a) on the NE edge of the profile, from 40 km onwards, seismicity hardly decreases; (b) between 30 and 40 km, below the Sierra Elvira and Granada fault traces, seismicity is concentrated mainly between 2 and 6 km depth; (c) toward the SW, the seismicity is more concentrated around 10 km depth. The January 2021 swarm accounts for most of the earthquakes recorded since 2000 (see histogram in Figure 7a). This swarm is located beneath Santa Fe at around 5 km depth (note the location of the focal mechanisms of earthquakes with Mw > 4.0; #21–25 in Table 1). The focal mechanisms are shifted slightly southwestwards of the NE shallow density maximum of the background seismicity (Figure 7c). Most of the focal mechanisms of the earthquakes having lower magnitude are projected to the northeast of the profile, and those of higher magnitude are projected southwestward. The earthquakes of higher magnitude (Mw > 3.5) have a more precise location, those with nodal planes between 45° and 60° are located at 2–6 km depth (in green in Figure 7), and those with a subhorizontal nodal plane have depths of 6, 7, and 12 km (in red in Figure 7).

The regional reduced stress tensor obtained from these solutions (Figure 7b) indicates a triaxial to prolate shape of the stress ellipsoid, supporting nearly NE-SW horizontal to radial extension. In addition, σ_1 is close to vertical, highly inclined toward the SW, for the most shallow 15 km of the crust. Stich et al. (2006) calculated a horizontal regional compression in the NW-SE direction, parallel to the shortening direction. Sparacino et al. (2020) presented an evidence supporting both NE-SW extension and NW-SE shortening. Despite the scarce availability of focal mechanisms, they serve to reveal the structure, to compute the stress regime, and to discuss the tectonic model.

6. High-Precision Leveling and Vertical Fault Displacements

The new geodetical leveling data may reveal the behavior of the active Granada Fault. In the Granada N line (Figure 8a; Movie S1), three sectors with very different styles of deformation appear. To the west of the line (J1–J4), there is a vertical displacement of up to -11 ± 2.5 mm in the period 1999–2009 (-1.1 ± 0.25 mm/yr), with a maximum rate of -5 ± 2.5 mm/yr during the first year. The deformation is accumulated between benchmarks J4 and J5, where the scarp associated with the Granada Fault is located. In the hangingwall block (J1–J4), a greater relative vertical displacement is observed when approaching to the fault. In the footwall block, benchmarks J5–J9 are relatively stable. In the eastern part of the line (J10–J16) lies a chaotic deformation, where occur maximum vertical displacements. In this sector, each of the points shows a different pattern (e.g., 10 ± 2.8 mm uplift in J10 or 8 ± 4.2 mm subsidence in J14). The acquired data in this area (J10–J16) may present more noise than in other places, since it is located on a slope of the Beiro River (Figure 8a), where shallow soil processes (ground settlement and landslides) are active. Therefore, they should be discarded from the tectonic interpretation.

The Granada S line (Figure 8b; Movie S2) documents a total vertical displacement of approximately 5 ± 0.9 mm between the years 1999–2013 (0.35 ± 0.06 mm/yr). Two clearly differentiated phases are seen in the deformation. The first one, during the years 1999–2009, shows an elevation of G2–G6 benchmarks amounting to 6 ± 0.9 mm (0.6 ± 0.09 mm/yr). Interestingly, vertical deformation of up to 3 ± 1.1 mm occurs in the period 1999–2000 only at benchmarks G2, G3, and G4, whereas until 2009, the deformation affected all the benchmarks, suggesting westward propagation of deformation. The second phase, 2009 to 2013, shows a relaxation of the terrain of up to 1 mm. During the two phases, the G7 and G8 benchmarks recorded very different behavior, probably due to local effects; hence they should be discarded when interpreting the tectonic deformation patterns.

The average rate of 1.1 ± 0.25 mm/yr measured for the time period 1999 to 2009 for Granada N is higher than that of the rate obtained for the Granada S line (0.35 ± 0.06 mm/yr), with both of them having substantially greater vertical displacement within the period 1999 to 2000 (Granada N, 5 ± 2.5 mm/yr and Granada S, 3 ± 1.1 mm/yr).

7. Discussion

The evolution of the Betic-Rif Cordillera and the surface uplift over the past 10 Ma is determined by NW-SE Eurasia-Nubia convergence. In this setting of continental collision (Ruiz-Constán et al., 2009), the western Betic Cordillera has undergone compression. The central Betic Cordillera is affected by regional compression with related uplift, in addition to an orthogonal extension. This extension produced mainly NW-SE normal faults, well developed in the Granada Basin, bounded to the east by the highest relief of Sierra Nevada (Sanz de Galdeano & Alfaro, 2004). The combination of geological fieldwork and geophysical techniques allows us to determine the structure of the faults and the basin, both at depth and at the surface. Moreover, the seismological data provide information about the activity and kinematics of faults at depth, while the geodetical data along the high-precision leveling lines constrain the surface deformation. Thus, by combining geological, geophysical, and geodetical studies of the active faults, the extensional mechanism and the relationship between shallow and deep structures can be identified.

7.1. Structure of the Sedimentary Infill and the Fault System of the Granada Basin

The residual gravity anomaly map (Figure 5c) and profiles (Figure 6) suggest that the Granada Basin Neogene-Quaternary sedimentary infill has a main anomaly minimum related to a depocenter near Granada city reaching 800–1,000 m below sea level. The Alfacar Fault, and especially the El Fargue and Granada faults, have facilitated subsidence of the depocenters in the eastern part of the basin since the Tortonian (Rodríguez-Fernández & Sanz de Galdeano, 2006), favoring the mainly northward tilting of the deposits, and determining the NE boundary of the anomaly. Given this framework, the Granada Basin can be described as a half-graben tilted toward the NNE that generates depocenters next to the main faults, as put forth for the northern part of the basin (Ruano et al., 2004), and now also evidenced in the eastern Granada Basin.

At the SE edge of the basin, the Trevenque Fault, the Dílar Fault, and farther south, the Padul Fault, extend toward the basement formed by the Alpujárride Complex, never affecting the Nevado-Filábride Complex (Galindo-Zaldívar et al., 1996). The contact between these metamorphic complexes is interpreted as the top-to-the-W extensional Mecina detachment, which was active during the lower Miocene (Jabaloy et al., 1992, 1993). This surface was folded by N-S compression, and therefore crops out in the Sierra Nevada and Sierra de Los Filabres antiforms (García-Dueñas et al., 1986). In the synforms, it would be located beneath the Neogene-Quaternary basins, including the Granada Basin. We suggest that the HANFs of the Granada Basin are connected with the Mecina detachment or another similar LANF.

The seismicity analysis reveals a great variety of dips for focal mechanisms in the shallowest crust, suggesting an interaction of HANFs and LANFs (Figure 9). Outcropping fault surfaces dip 50°–60°, in agreement with the highest magnitude earthquake shallow focal solutions (45°–60°; green in Figures 7 and 9). Earthquakes of Mw > 3.5 with one low-angle nodal plane focal mechanism (red in Figures 7 and 9) are located at depths between 6 and 12 km, W-SW of the main SW-dipping faults. They could be related to an active extensional deformation zone, although considering the depth error and its low magnitude, they cannot be associated with any specific structure (Figure 9c). In fact, there is a sudden decrease of earthquakes below 11–12 km depth (Figure 7c), where HANFs could be rooted. The sparsity of earthquakes could also be due to termination of the seismogenic layer, which is usually 10–15 km thick in areas undergoing extension (Chen & Molnar, 1983). Although previous seismic and seismic tomography studies to the SW of the Granada Basin situate the limit of the seismogenic layer around 17 or 18 km depth, we cannot discard that in our study area, it lies at a depth of around 12 km, given the relatively poor resolution. Thus, with the provided data—subhorizontal nodal planes of the focal mechanisms (e.g., #13, 14, 18, 20)—we can merely interpret the presence of a detachment that separates two blocks of different deformation: (a) a brittle hangingwall, where antithetic faults (e.g., the Santa Fe and Belicena-Alhendín faults) dipping toward the NW and the conjugate faults of Sierra Elvira are located, and (b) a footwall that is either undeformed or affected by ductile shearing. Seismicity research on the whole Granada Basin (Morales et al., 1997) shows that seismicity increases with depth in the SW sector of the basin, outside the study zone, suggesting the SW-ward dipping of LANFs (Figures 7c and 9) (Galindo-Zaldívar et al., 1999). Crustal models in the central Betic Cordillera propose that a detachment separates the Betic and the Iberian crusts at around 10–15 km depth (Galindo-Zaldívar et al., 1997; Mancilla et al., 2015). Therefore, LANFs could be rooted at the boundary between the two crusts, facilitating extension at shallow crustal levels in the central Betic Cordillera (Galindo-Zaldívar et al., 2015). Indeed, deep seismic reflection profiles that cut across the Internal Zones 30 km east of the study region (Galindo-Zaldívar et al., 1997), the seismic refraction profiles that intersect the seismic reflection profiles and cross the study area (Banda et al., 1993), and magnetotelluric data (Pous et al., 1995) suggest the existence of crustal detachment levels at depths from 10 to 20 km. These results are in agreement with previous studies of the sedimentary infill of Granada Basin based on seismic profiles (Morales et al., 1990; Rodríguez-Fernández & Sanz de Galdeano, 2006; Sanz de Galdeano et al., 2003, 2012), which now extend into the basement.

The Mecina Extensional System, which affects the Sierra Nevada, is considered to have been active from Burdigalian to Early Tortonian time (Jabaloy et al., 1992; Vissers et al., 1995). The geological data east of the Granada Basin indicate that the HANFs are connected with the top-to-the-WSW Mecina extensional detachment that was further reactivated in the western Sierra Nevada (Galindo-Zaldívar et al., 1996). The current data moreover suggest that it, or a similar LANF, may be active at depth further west below the Granada Basin, in continuity with the HANF. Future studies may fine-tune the role of this LANF in the extension of the Central Betic Cordillera. The associated earthquakes do not exceed Mw 4.0, suggesting that seismic ruptures affect a sector a few hundred meters long and entail a few millimeters of displacement. The extension could be accommodated by creep or by other large earthquakes not occurring in the instrumental or historical period. Indeed, large earthquakes on LANFs (e.g., Woodlark Basin, Abers et al., 1997) can have long recurrence periods (Wernicke, 1995), and stable creeping fault segments in some cases become unstable owing to the rapid shear heating of pore fluids (Noda & Lapusta, 2013).

7.2. Activity of the Main Faults of the Northeastern Granada Basin

Several factors have to be taken into account when dealing with leveling data. The lines are located with the best orientation to intersect the main Granada fault, and benchmarks were installed in the most stable places on structures old enough to be well settled. The NE part of the Granada N line has been affected by landslides and was excluded from the tectonic interpretation. The other benchmarks are located in areas of low slopes; hence the influence of landslides should not be important. The absence of close water boreholes suggests that all the benchmarks are affected in a similar way by water table fluctuations. Moreover, the highest vertical displacements are located close to the fault traces, suggesting a mainly tectonic origin.

The two leveling lines present common characteristics (Figure 8). There is uplift of the NE block (footwall) and subsidence of the SW block (hangingwall). In addition, both profiles show higher rates for the 1999 to 2000 period. The similarities also support that the observed vertical displacements are related to the Granada Fault activity. In the Granada N high-precision leveling line (Figure 8c), the fault reaches the surface and creates a single scarp, where we quantified an average vertical displacement rate of 1.1 mm/yr (Figure 8a). In the Granada S line (Figure 8b), vertical displacements affect a wide zone with average rate of 0.35 mm/yr. This deformation pattern may correspond to a drape fold related to the activity of blind faults, similar to that proposed by Keller et al. (1996) below the La Zubia alluvial fan, found south of the Granada S line. The Granada Fault is branched southward, developing a wide deformed area (Figures 4 and 8b; Azañón et al., 2004). Therefore, along the Granada S high-precision leveling line, only some of the deformation of the entire fault zone is determined, in agreement with the lower vertical displacement rates.

The new geophysical and geodetic data presented in this paper reveal that the NE zone's faults are currently or recently active. These data are consistent with previous geomorphic (Carvajal & Sanz de Galdeano, 2001; Pérez-Peña et al., 2015; among others) and paleoseismic (Sanz de Galdeano et al., 2003, 2012) research findings. For one, it is an area with a high seismicity rate (Figure 7), especially for the hangingwall of the Granada Fault and Sierra Elvira faults, and somewhat less for the hangingwall of the El Fargue Fault. Toward the NE, this activity decreases drastically before reaching the Alfacar Fault. Second, all the geomorphic indexes point to a recent fault activity and relative uplift of the footwall of the Granada Fault: (a) hypsometric integral studies assign high values to the footwall of the Granada fault (Pérez-Peña, Azañón, Booth-Rea, et al., 2009), meaning uplift related to fault activity; (b) the new geodetic data are consistent with studies on incision rates carried out in the same place, 0.45 mm/yr (Pérez-Peña et al., 2015) and 0.8 mm/yr (Carvajal & Sanz de Galdeano, 2001) in the footwall of the Granada Fault; (c) analysis of the SLk index (Pérez-Peña, Azañón, Azor, et al., 2009) gives positive anomalies when the rivers cross the Alfacar and Granada Faults; (d) whereas the Alfacar and Granada Faults have scarps reaching hundreds of meters (Figure 4d), the El Fargue Fault however, has a minor scarp (Figures 2b and 4d). The SLk anomalies and the scarp of the Alfacar Fault could be due to lithological changes between the basement carbonates and the detritic sediments of the sedimentary infill. In the Granada Fault, these geomorphic features are likely related to tectonic activity, since the lithology of the hangingwall and the footwall are similar. The two high-precision leveling lines demonstrate that the Granada Fault is currently active, with average rates of vertical displacements between 0.35 and 1.1 mm/yr, in agreement with geomorphological slip rates. All the evidence underlines the current and important activity of the Granada Fault. The faults located toward the NE do not show much activity, however, in agreement with previous paleoseismological studies (Sanz de Galdeano et al., 2003, 2012). The El Fargue fault produces a small scarp and could have some associated seismicity, but it does not present SLk anomalies (Pérez-Peña, Azañón, Azor, et al., 2009). In turn, the Alfacar Fault does not present associated seismicity and is covered by sediments that are locally up to 4 m thick. Although it presents anomalous SLk values, they are at least partly associated with lithological changes.

Both short-term deformation (the geodetical leveling data from two high-precision leveling lines) and long-term deformation (geological and geomorphological fault slip rates) should be constrained for adequate monitoring of the fault activity. Still, geodetically recorded slip rates are not always representative of the longer-term geologically derived rates. There are several examples of such discrepancies in other extensional settings worldwide such as the Basin and Range (Friedrich et al., 2003) and the central Apennines (Papanikolaou et al., 2005). The vertical-displacement values obtained from high-precision leveling lines of the Granada Fault are considerably higher than those obtained from the geological studies by Sanz de Galdeano et al. (2003) (0.38 mm/yr; from 300 m displacement observed in the last 0.8 Ma), Sanz de

Galdeano et al. (2012) (0.1 mm/yr for the last 2.5 Ma) and Azañón et al. (2013) (0.003 mm/yr). The values are, however, more similar to the incision rates obtained from geomorphic analyses by Carvajal and Sanz de Galdeano (2001) (0.8 mm/yr) and Pérez-Peña et al. (2015) (0.45 mm/yr). Vertical displacement rates fluctuate significantly from year to year. Although high-precision leveling profiles indicate average vertical displacement, those average rates do not occur continuously; stages with higher rates (e.g., 1999–2000) or deformation relaxation (2009–2013) should be differentiated. The high-rate stages cannot be considered as coseismic deformation, since they are not temporally related to increases in seismicity. They might be related to progressive propagation of the deformation toward the surface related to previous seismic events at depth. The higher values of the Granada N line with respect to the geomorphological values could be related to the influence of other factors besides tectonics. On the other hand, it could also be linked to the fact that geological studies cover large periods of diverse activity, whereas geodetical studies are conducted on tectonically active structures. Therefore, the Granada Fault, despite its currently higher modern vertical displacement rates, is likely to have been much less active in other geological periods. Other faults of the basin may have been the active ones.

The average vertical-displacement rates of the Granada Fault are in line with those determined for other faults of the central Betic Cordillera. Gil et al. (2017) computed a 0.78 ± 0.08 mm/yr rate for the Padul Fault, considering horizontal GPS displacements of 0.5 ± 0.05 mm/yr and an average 55° dip. Similarly, Reinhardt et al. (2007) calculated a 0.4–0.8 mm/yr relative uplift in the footwall of the Padul Fault from geomorphic observations. The Balanegra Fault presents lower average values (0.14 mm/yr) because extension is distributed on other faults of El Campo de Dalías (Galindo-Zaldívar et al., 2013). At any rate, it is remarkable that the Granada S line shows a late episode of reverse deformation, similar to the Balanegra Fault (Galindo-Zaldívar et al., 2013), most likely due to the recovery to some extent of accumulated elastic deformation events.

The Granada Fault, together with the Padul Fault, appear to be the main structures accommodating extension in the central Betic Cordillera. Considering an average dip angle of 30° and a direction of N150°E for the Granada Fault, a horizontal displacement between 0.6 ± 0.1 and 1.9 ± 0.43 mm/yr in the N240°E direction is obtained. The CGPS stations located in the eastern and western Granada Basin, GRA1 (0.94 ± 0.35 mm/yr) and LOJA (2.84 ± 0.35 mm/yr) (Galindo-Zaldívar et al., 2015; Figure 1), document extension of 1.9 ± 0.35 mm/yr. Accordingly, the Granada Fault may be responsible for most of the present extension that occurs in the whole Granada Basin.

7.3. Geodynamic Implications

The causes of the present extension of the central Betic Cordillera and the recent evolution of the Betics have been the subject of debate in recent decades. Subduction with or without rollback and delamination processes have been proposed (Brun & Faccenna, 2008; Mancilla et al., 2013; Ruiz-Constán et al., 2012; among others). Most authors agree that subduction—although in transition to collision—is still active, producing slab rollback (González-Castillo et al., 2015; Pedrera et al., 2011; Ruiz-Constán et al., 2011; Wortel & Spakman, 2000) that may induce extension in the hinterland. In addition, indentation and uplift in the central-eastern zone may produce orogenic collapse and westward escape tectonics, as occurs in the eastern Betic Cordillera (Silva et al., 1993), in the Alboran Sea (Estrada et al., 2018), and in the Rif (Chalouan et al., 2006). Still other proposals (Mancilla et al., 2015; Spakman et al., 2018) support delamination combined with the detaching or tear-faulting of Iberian subducting crust in the central Betic Cordillera as the cause of the extension. The stress tensor, in the central Betic Cordillera, shows reverse σ_1 and σ_2 at the uppermost crust (<15 km) (Sparacino et al., 2020; Stich et al., 2006). Maximum compression (σ_1) becomes vertical due to the large uplift (Braga et al., 2003) and suggests the occurrence of gravitational collapse of the thickened crust. The well-directed NE-SW trend of extension in the upper crust related to the rollback tectonics of the Gibraltar Arc (González-Castillo et al., 2015), together with the former collapse, would have produced the high- and low-angle extensional system. This scenario, in addition to the NW-SE shortening, is consistent with σ_3 in NE-SW direction.

HANF and LANF systems commonly accommodate orogen-parallel extension. The Granada Basin fault system shares features with the Brenner Fault in the eastern Alps (Selverstone, 1988). The Brenner Fault separates areas of the distinct trend and intensity of tectonic deformation (Rosenberg & García, 2011), and seismic activity normally does not exceed earthquakes with magnitude Mw 3.0 in an area undergoing

horizontal displacement of 0.5 mm/yr (Reiter et al., 2005). There are similarities with the LANFs proposed in the Gulf of Corinth (Chiaraluce et al., 2004; Rigo et al., 1996) and Alto Tiberina Fault (Gualandi et al., 2017). These low-angle extensional zones have associated seismicity not exceeding Mw 4.0. The highest magnitude events occur on the HANFs of the hangingwall (Boncio et al., 2004). However, the seismicity recorded in instrumental and historical periods of the above scenarios is far from the Mw 6.3 and 6.7 earthquakes (Abers et al., 1997), and larger events that possibly took place during the Holocene in Woodlark Basin (Biemiller et al., 2020).

8. Conclusions

The integration of field geology, geophysical, and geodetical studies allows us to constrain the structure and activity of the extensional fault system in the NE Granada half-graben, located in the central Betic Cordillera. This basin is deformed by HANFs, mainly dipping toward the SW, connected with a low-angle extensional deformation zone reaching 11–12 km in depth.

The active faults in the NE sector tilted the deposits toward the N-NE, developing depocenters. Toward the surface (<6 km depth), the HANFs (60°) are responsible for much of the shallower seismicity and larger events (e.g., earthquakes related to the January 2021 swarm). At greater depths (6–12 km), earthquakes suggest an active subhorizontal extensional deformation zone.

The Granada Fault, together with the Sierra Elvira faults, is the main fault of the system, showing activity supported by the vertical displacements observed in the high-precision leveling lines (average rates of 0.35–1.1 mm/yr), seismicity, and earthquake focal mechanism solutions. At the surface, it changes in character and activity along strike. A fault scarp has developed in the northern area, while toward the south it becomes a blind fault.

Ultimately, the high- and low-angle fault system of the Granada Basin could be an active segment related to the Mecina Extensional System. At present, the fault system facilitates extension in the upper crust of the central zone of the Betic Cordillera—produced by the displacement toward the W of the Gibraltar Arc related to rollback tectonics—in addition to rock uplift related to NW-SE compression.

Data Availability Statement

The seismicity data are available on the IGN website at http://www.ign.es/web/ign/portal/sis-catalogo-terremotos and https://www.ign.es/web/ign/portal/tensor-momento-sismico/. The DTM used in the topographic correction, topographic profiles, and geologic maps is available in http://centrodedescargas.cnig.es/CentroDescargas/index.jsp. The information about gravity bases of IGN is provided at https://www.ign.es/web/ign/portal/grv-gravedad-absoluta. The Bouguer anomaly data from the TopoIberia project are accessible on the website http://info.igme.es/SIGEOF/. Finally, fault data were obtained from the Quaternary Faults Database of Iberia at https://info.igme.es/qafi/.

References

Abers, G. A. (1991). Possible seismogenic shallow-dipping normal faults in the Woodlark-D'Entrecasteaux extensional province, Papua New Guinea. *Geology*, *19*(12), 1205–1208. https://doi.org/10.1130/0091-7613(1991)019%3C1205:PSSDNF%3E2.3.CO;2

Abers, G. A., Mutter, C. Z., & Fang, J. (1997). Shallow dips of normal faults during rapid extension: Earthquakes in the Woodlark-D'Entrecasteaux rift system, Papua New Guinea. *Journal of Geophysical Research*, *102*(B7), 15301–15317. https://doi.org/10.1029/97JB00787

Absolute gravity. (2021). Retrieved from https://www.ign.es/web/ign/portal/grv-gravedad-absoluta

Alfaro, P., Delgado, J., Sanz de Galdeano, C., Galindo-Zaldívar, J., García-Tortosa, F. J., López-Garrido, A. C., et al. (2008). The Baza Fault: A major active extensional fault in the central Betic Cordillera (south Spain). *International Journal of Earth Sciences*, *97*(6), 1353–1365. https://doi.org/10.1007/s00531-007-0213-z

Anderlini, L., Serpelloni, E., & Belardinelli, M. E. (2016). Creep and locking of a low-angle normal fault: Insights from the Altotiberina fault in the Northern Apennines (Italy). *Geophysical Research Letters*, *43*(9), 4321–4329. https://doi.org/10.1002/2016GL068604

Anderson, E. M. (1951). *The dynamics of faulting and dyke formation: With applications to Britain* (2nd ed.). Oliver and Boyd.

Araña, V., & Vegas, R. (1974). Plate tectonics and volcanism in the Gibraltar arc. *Tectonophysics*, *24*(3), 197–212. https://doi.org/10.1016/0040-1951(74)90008-0

Ayala, C., Bohoyo, F., Maestro, A., Reguera, M. I., Torne, M., Rubio, F., et al. (2016). Updated Bouguer anomalies of the Iberian Peninsula: A new perspective to interpret the regional geology. *Journal of Maps*, *12*(5), 1089–1092. https://doi.org/10.1080/17445647.2015.1126538

Azañón, J. M., Azor, A., Booth-Rea, G., & Torcal, F. (2004). Small-scale faulting, topographic steps and seismic ruptures in the Alhambra (Granada, southeast Spain). *Journal of Quaternary Science*, *19*(3), 219–227. https://doi.org/10.1002/jqs.838

Azañón, J. M., García-Mayordomo, J., Insua, J. M., & Rodríguez-Peces, M. J. (2013). Seismic hazard of the Granada Fault. *Cuaternario y Geomorfologia*, *27*(3–4), 5–32.

Banda, E., Gallart, J., García-Dueñas, V., Dañobeitia, J. J., & Makris, J. (1993). Lateral variation of the crust in the Iberian peninsula: New evidence from the Betic Cordillera. *Tectonophysics*, *221*(1), 53–66. https://doi.org/10.1016/0040-1951(93)90027-H

Benedetti, L., Finkel, R., Papanastassiou, D., King, G., Armijo, R., Ryerson, F., et al. (2002). Post-glacial slip history of the Sparta fault (Greece) determined by 36Cl cosmogenic dating: Evidence for non-periodic earthquakes. *Geophysical Research Letters*, *29*(8), 87–91. https://doi.org/10.1029/2001GL014510

Biemiller, J., Taylor, F., Lavier, L., Yu, T. L., Wallace, L., & Shen, C. C. (2020). Emerged coral reefs record holocene low-angle normal fault earthquakes. *Geophysical Research Letters*, *47*(20), e2020GL089301. https://doi.org/10.1029/2020GL089301

Blanco, M. J., & Spakman, W. (1993). The P-wave velocity structure of the mantle below the Iberian Peninsula: Evidence for subducted lithosphere below southern Spain. *Tectonophysics*, *221*(1), 13–34. https://doi.org/10.1016/0040-1951(93)90025-F

Boncio, P., Lavecchia, G., & Pace, B. (2004). Defining a model of 3D seismogenic sources for Seismic Hazard Assessment applications: The case of central Apennines (Italy). *Journal of Seismology*, *8*(3), 407–425. https://doi.org/10.1023/B:JOSE.0000038449.78801.05

Braga, J. C., Martín, J. M., & Quesada, C. (2003). Patterns and average rates of late Neogene–Recent uplift of the Betic Cordillera, SE Spain. *Geomorphology*, *50*(1–3), 3–26. https://doi.org/10.1016/S0169-555X(02)00205-2

Brun, J. P., & Faccenna, C. (2008). Exhumation of high-pressure rocks driven by slab rollback. *Earth and Planetary Science Letters*, *272*(1–2), 1–7. https://doi.org/10.1016/j.epsl.2008.02.038

Buforn, E., Bezzeghoud, M., Udias, A., & Pro, C. (2004). Seismic sources on the Iberia-African plate boundary and their tectonic implications. *Pure and Applied Geophysics*, *161*(3), 623–646. https://doi.org/10.1007/s00024-003-2466-1

Buforn, E., Pro, C., Cesca, S., Udias, A., & Del Fresno, C. (2011). The 2010 Granada, Spain, deep earthquake. *Bulletin of the Seismological Society of America*, *101*(5), 2418–2430. https://doi.org/10.1785/0120110022

Calvert, A., Sandvol, E., Seber, D., Barazangi, M., Vidal, F., Alguacil, G., & Jabour, N. (2000). Propagation of regional seismic phases (Lg and Sn) and Pn velocity structure along the Africa–Iberia plate boundary zone: Tectonic implications. *Geophysical Journal International*, *142*(2), 384–408. https://doi.org/10.1046/j.1365-246x.2000.00160.x

Carvajal, R., & Sanz de Galdeano, C. (2001). La red de drenaje de la rednororiental de la Cuenca de Granada. Del río Bermejo al Darro. Aplicación de índices geomorfológicos. In C. Sanz de Galdeano, J. A. Peláez, & A. C. López Garrido (Eds.), *La Cuenca de Granada. Estructura, Tectónica Activa, Sismicidad, Geomorfología y Dataciones Existentes* (pp. 67–77). University of Granada.

Chalouan, A., Galindo-Zaldívar, J., Akil, M., Marín, C., Chabli, A., Ruano, P., et al. (2006). Tectonic wedge escape in the southwestern front of the Rif Cordillera (Morocco). In G. Moratti, & A. Chalouan (Eds.), *Tectonics of the Western Mediterranean and North Africa* (pp. 101–118). Geological Society of London. https://doi.org/10.1144/gsl.sp.2006.262.01.06

Chen, W. P., & Molnar, P. (1983). Focal depths of intracontinental and intraplate earthquakes and their implications for the thermal and mechanical properties of the lithosphere. *Journal of Geophysical Research*, *88*(B5), 4183–4214. https://doi.org/10.1029/JB088iB05p04183

Chertova, M. V., Spakman, W., Geenen, T., van den Berg, A. P., & van Hinsbergen, D. J. J. (2014). Underpinning tectonic reconstructions of the western Mediterranean region with dynamic slab evolution from 3-D numerical modelling. *Journal of Geophysical Research: Solid Earth*, *119*, 5876–5902. https://doi.org/10.1002/2014JB011150

Chiaraluce, L., Amato, A., Cocco, M., Chiarabba, C., Selvaggi, G., Di Bona, M., et al. (2004). Complex normal faulting in the Apennines thrust-and-fold belt: The 1997 seismic sequence in central Italy. *Bulletin of the Seismological Society of America*, *94*(1), 99–116. https://doi.org/10.1785/0120020052

Chiaraluce, L., Chiarabba, C., Collettini, C., Piccinini, D., & Cocco, M. (2007). Architecture and mechanics of an active low-angle normal fault: Alto Tiberina fault, northern Apennines, Italy. *Journal of Geophysical Research*, *112*(B10). https://doi.org/10.1029/2007JB005015

CNIG. (2021). *Download center of National Center of Geographic Information (CNIG)*. IGN. Retrieved from http://centrodedescargas.cnig.es/CentroDescargas/index.jsp

Collettini, C. (2011). The mechanical paradox of low-angle normal faults: Current understanding and open questions. *Tectonophysics*, *510*(3–4), 253–268. https://doi.org/10.1016/j.tecto.2011.07.015

Collettini, C., & Holdsworth, R. E. (2004). Fault zone weakening and character of slip along low-angle normal faults: Insights from the Zuccale fault, Elba, Italy. *Journal of the Geological Society*, *161*(6), 1039–1051. https://doi.org/10.1144/0016-764903-179

Collettini, C., & Sibson, R. H. (2001). Normal faults, normal friction? *Geology*, *29*(10), 927–930. https://doi.org/10.1130/0091-7613(2001)029<0927:NFNF>2.0.CO;2

Cowie, P. A., Phillips, R. J., Roberts, G. P., McCaffrey, K., Zijerveld, L. J. J., Gregory, L. C., et al. (2017). Orogen-scale uplift in the central Italian Apennines drives episodic behaviour of earthquake faults. *Scientific Reports*, *7*, 44858. https://doi.org/10.1038/srep44858

de Jong, K. (1991). *Tectonometamorphic studies and radiometric dating in the Betic cordilleras (SE Spain): With implications for the dynamics of extension and compression in the western Mediterranean area* (Doctoral dissertation). Vrije Universiteit Amsterdam.

de Jong, K. (1993). The tectono-metamorphic and chronologic development of the Betic Zone (SE Spain) with implications for the geodynamic evolution of the western Mediterranean area. *Verhandelingen der Koninklijke Nederlandsche Akademie van Wetenschappen*, *96*, 295–333.

DeMets, C., Gordon, R. G., & Argus, D. F. (2010). Geologically current plate motions. *Geophysical Journal International*, *181*(1), 1–80. https://doi.org/10.1111/j.1365-246X.2009.04491.x

Estrada, F., Galindo-Zaldívar, J., Vázquez, J. T., Ercilla, G., D'Acremont, E., Alonso, B., & Gorini, C. (2018). Tectonic indentation in the central Alboran Sea (westernmost Mediterranean). *Terra Nova*, *30*(1), 24–33. https://doi.org/10.1111/ter.12304

Fadil, A., Vernant, P., McClusky, S., Reilinger, R., Gomez, F., Ben Sari, D., et al. (2006). Active tectonics of the western Mediterranean: Geodetic evidence for rollback of a delaminated subcontinental lithospheric slab beneath the Rif Mountains, Morocco. *Geology*, *34*(7), 529–532. https://doi.org/10.1130/G22291.1

Fernández, J., & Rodríguez-Fernández, J. (1991). Facies evolution of nearshore marine clastic deposits during the Tortonian transgression—Granada Basin, Betic Cordilleras, Spain. *Sedimentary Geology*, *71*(1–2), 5–21. https://doi.org/10.1016/0037-0738(91)90003-V

Floyd, J. S., Mutter, J. C., Goodliffe, A. M., & Taylor, B. (2001). Evidence for fault weakness and fluid flow within an active low-angle normal fault. *Nature*, *411*(6839), 779–783. https://doi.org/10.1038/35081040

Friedrich, A. M., Wernicke, B. P., Niemi, N. A., Bennett, R. A., & Davis, J. L. (2003). Comparison of geodetic and geologic data from the Wasatch region, Utah, and implications for the spectral character of Earth deformation at periods of 10 to 10 million years. *Journal of Geophysical Research*, *108*(B4). https://doi.org/10.1029/2001JB000682

Galindo-Zaldívar, J., Borque, M. J., Pedrera, A., Marín-Lechado, C., Gil, A. J., & López-Garrido, A. C. (2013). Deformation behaviour of the low-rate active Balanegra Fault Zone from high-precision levelling (Betic Cordillera, SE Spain). *Journal of Geodynamics*, *71*, 43–51. https://doi.org/10.1016/j.jog.2013.07.003

Galindo-Zaldívar, J., Gil, A. J., Borque, M. J., González-Lodeiro, F., Jabaloy, A., Marín-Lechado, C., et al. (2003). Active faulting in the internal zones of the central Betic Cordilleras (SE, Spain). *Journal of Geodynamics*, *36*(1–2), 239–250. https://doi.org/10.1016/S0264-3707(03)00049-8

Galindo-Zaldívar, J., Gil, A. J., Sanz de Galdeano, C., de Lacy, M. C., García-Armenteros, J. A., et al. (2015). Active shallow extension in central and eastern Betic Cordillera from CGPS data. *Tectonophysics*, *663*, 290–301. https://doi.org/10.1016/j.tecto.2015.08.035

Galindo-Zaldívar, J., González-Lodeiro, F., & Jabaloy, A. (1989). Progressive extensional shear structures in a detachment contact in the Western Sierra Nevada (Betic Cordilleras, Spain). *Geodinamica Acta*, *3*(1), 73–85. https://doi.org/10.1080/09853111.1989.11105175

Galindo-Zaldívar, J., González-Lodeiro, F., & Jabaloy, A. (1993). Stress and palaeostress in the Betic-Rif cordilleras (Miocene to the present). *Tectonophysics*, *227*(1–4), 105–126. https://doi.org/10.1016/0040-1951(93)90090-7

Galindo-Zaldívar, J., Jabaloy, A., & Gonzalez-Lodeiro, F. (1996). Reactivation du detachement extensif de Mecina dans le secteur occidental de la Sierra Nevada (Cordilleres Betiques, SE de l'Espagne). *Comptes Rendus de l'Academie des Sciences-Serie IIa-Sciences de la Terre et des Planetes*, *323*(7), 615–622.

Galindo-Zaldívar, J., Jabaloy, A., González-Lodeiro, F., & Aldaya, F. (1997). Crustal structure of the central sector of the Betic Cordillera (SE Spain). *Tectonics*, *16*(1), 18–37. https://doi.org/10.1029/96TC02359

Galindo-Zaldívar, J., Jabaloy, A., Serrano, I., Morales, J., González-Lodeiro, F., & Torcal, F. (1999). Recent and present-day stresses in the Granada Basin (Betic Cordilleras): Example of a late Miocene-present-day extensional basin in a convergent plate boundary. *Tectonics*, *18*(4), 686–702. https://doi.org/10.1029/1999TC900016

Garate, J., Martin-Davila, J., Khazaradze, G., Echeverria, A., Asensio, E., Gil, A. J., et al. (2015). Topo-Iberia project: CGPS crustal velocity field in the Iberian Peninsula and Morocco. *GPS Solutions*, *19*(2), 287–295. https://doi.org/10.1007/s10291-014-0387-3

García-Dueñas, V., Balanyá, J. C., & Martínez-Martínez, J. M. (1992). Miocene extensional detachments in the outcropping basement of the northern Alboran basin (Betics) and their tectonic implications. *Geo-Marine Letters*, *12*(2–3), 88–95. https://doi.org/10.1007/BF02084917

García-Dueñas, V., Martínez-Martínez, J. M., & Navarro-Vilá, F. (1986). La zona de falla de Torres Cartas, conjunto de fallas normales de bajo-ángulo entre Nevado-Filábres y Alpujárrides (Sierra de Alhamilla, Béticas Orientales). *Geogaceta*, *1*, 17–19. Retrieved from http://hdl.handle.net/10272/18499

García-Mayordomo, J., Insua-Arévalo, J. M., Martínez-Díaz, J. J., Jiménez-Díaz, A., Martín-Banda, R., Martín-Alfageme, S., et al. (2012). The Quaternary faults database of Iberia (QAFI v.2.0). *Journal of Iberian Geology*, *38*(1), 285–302. https://doi.org/10.5209/rev_jige.2012.v38.n1.39219

Gil, A. J., Galindo-Zaldívar, J., Sanz de Galdeano, C., Borque, M. J., Sánchez-Alzola, A., Martínez-Martos, M., & Alfaro, P. (2017). The Padul normal fault activity constrained by GPS data: Brittle extension orthogonal to folding in the central Betic Cordillera. *Tectonophysics*, *712*, 64–71. https://doi.org/10.1016/j.tecto.2017.05.008

Gill, R. C. O., Aparicio, A., El Azzouzi, M., Hernandez, J., Thirlwall, M. F., Bourgois, J., & Marriner, G. F. (2004). Depleted arc volcanism in the Alboran Sea and shoshonitic volcanism in Morocco: Geochemical and isotopic constraints on Neogene tectonic processes. *Lithos*, *78*(4), 363–388. https://doi.org/10.1016/j.lithos.2004.07.002

Giménez, J., Borque, M. J., Gil, A. J., Alfaro, P., Estévez, A., & Suriñach, E. (2009). Comparison of long-term and short-term uplift rates along an active blind reverse fault zone (Bajo Segura, SE Spain). *Studia Geophysica et Geodaetica*, *53*(1), 81–98. https://doi.org/10.1007/s11200-009-0005-y

González, A. (2017). The Spanish national earthquake catalogue: Evolution, precision and completeness. *Journal of Seismology*, *21*(3), 435–471. https://doi.org/10.1007/s10950-016-9610-8

González-Castillo, L., Galindo-Zaldívar, J., de Lacy, M. C., Borque, M. J., Martínez-Moreno, F. J., et al. (2015). Active rollback in the Gibraltar Arc: Evidences from CGPS data in the western Betic Cordillera. *Tectonophysics*, *663*, 310–321. https://doi.org/10.1016/j.tecto.2015.03.010

Grobe, A., von Hagke, C., Littke, R., Dunkl, I., Wübbeler, F., Muchez, P., & Urai, J. L. (2019). Tectono-thermal evolution of Oman's Mesozoic passive continental margin under the obducting Semail Ophiolite: A case study of Jebel Akhdar, Oman. *Solid Earth*, *10*(1), 149–175. https://doi.org/10.5194/se-10-149-2019

Gualandi, A., Nichele, C., Serpelloni, E., Chiaraluce, L., Anderlini, L., Latorre, D., et al. (2017). Aseismic deformation associated with an earthquake swarm in the northern Apennines (Italy). *Geophysical Research Letters*, *44*(15), 7706–7714. https://doi.org/10.1002/2017GL073687

Hayman, N. W., Knott, J. R., Cowan, D. S., Nemser, E., & Sarna-Wojcicki, A. M. (2003). Quaternary low-angle slip on detachment faults in Death Valley, California. *Geology*, *31*(4), 343–346. https://doi.org/10.1130/0091-7613(2003)031%3C0343:QLASOD%3E2.0.CO;2

Herraiz, M., De Vicente, G., Lindo, R., Giner, J., Simón, J. L., González Casado, J. M., et al. (1998). Proyecto Sigma. Análisis del estado de esfuerzos tectónicos reciente y actual en la Península Ibérica. *Colección Otros Documentos*, (Vol. 10). Consejo de Seguridad Nuclear.

Hinze, W. J. (2003). Bouguer reduction density, why 2.67? *Geophysics*, *68*(5), 1559–1560. https://doi.org/10.1190/1.1620629

Hoernle, K., van den Bogaard, P., Duggen, S., Mocek, B., & Garbe-Schönberg, D. (1999). Evidence for Miocene subduction beneath the Alboran Sea (Western Mediterranean) from 40Ar/39Ar age dating and the geochemistry of volcanic rocks from holes 977A and 978A. *Proceeding of the Ocean Drilling Program, Scientific Results*, *161*, 301–305. https://doi.org/10.2973/odp.proc.sr.161.264.1999

Houseman, G. A., McKenzie, D. P., & Molnar, P. (1981). Convective instability of a thickened boundary layer and its relevance for the thermal evolution of continental convergent belts. *Journal of Geophysical Research*, *86*(B7), 6115–6132. https://doi.org/10.1029/JB086iB07p06115

Hreinsdóttir, S., & Bennett, R. A. (2009). Active aseismic creep on the Alto Tiberina low-angle normal fault, Italy. *Geology*, *37*(8), 683–686. https://doi.org/10.1130/G30194A.1

Iribarren, L., Vergés, J., Camurri, F., Fullea, J., & Fernández, M. (2007). The structure of the Atlantic–Mediterranean transition zone from the Alboran Sea to the Horseshoe Abyssal Plain (Iberia–Africa plate boundary). *Marine Geology*, *243*(1–4), 97–119. https://doi.org/10.1016/j.margeo.2007.05.011

Jabaloy, A., Galindo-Zaldívar, J., & González-Lodeiro, F. (1992). The Mecina extensional system: Its relation with the post-Aquitanian piggy-back basins and the paleostresses evolution (Betic Cordilleras, Spain). *Geo-Marine Letters*, *12*(2–3), 96–103. https://doi.org/10.1007/BF02084918

Jabaloy, A., Galindo-Zaldívar, J., & González-Lodeiro, F. (1993). The Alpujárride-Nevado-Fibábride extensional shear zone, Betic Cordillera, SE Spain. *Journal of Structural Geology*, *15*(3–5), 555–569. https://doi.org/10.1016/0191-8141(93)90148-4

Jackson, J. A., & White, N. J. (1989). Normal faulting in the upper continental crust: Observations from regions of active extension. *Journal of Structural Geology*, *11*(1–2), 15–36. https://doi.org/10.1016/0191-8141(89)90033-3

Jolivet, L., Lecomte, E., Huet, B., Denèle, Y., Lacombe, O., Labrousse, L., et al. (2010). The north cycladic detachment system. *Earth and Planetary Science Letters*, *289*(1–2), 87–104. https://doi.org/10.1016/j.epsl.2009.10.032

Kane, M. F. (1962). A comprehensive system of terrain corrections using a digital computer. *Geophysics*, *27*(4), 455–462. https://doi.org/10.1190/1.1439044

Keller, E. A., Sanz de Galdeano, C., & Chacón, J. (1996). *Tectonic geomorphology and earthquake hazard of Sierra Nevada, Southern Spain*. Paper presented at 1st Conferencia Internacional Sierra Nevada.

Koulali, A., Ouazar, D., Tahayt, A., King, R. W., Vernant, P., Reilinger, R. E., et al. (2011). New GPS constraints on active deformation along the Africa–Iberia plate boundary. *Earth and Planetary Science Letters*, *308*(1–2), 211–217. https://doi.org/10.1016/j.epsl.2011.05.048

Lonergan, L., & White, N. (1997). Origin of the Betic-Rif mountain belt. *Tectonics*, *16*(3), 504–522. https://doi.org/10.1029/96TC03937

Lupiani, E., & Soria, J. (1988). *Mapa geológico de España a escala 1:50.000. Hoja número 1009 (Granada)*. Insituto Geológico y Minero de España.

Mancilla, F. L., Booth-Rea, G., Stich, D., Pérez-Peña, J. V., Morales, J., Azañón, J. M., et al. (2015). Slab rupture and delamination under the Betics and Rif constrained from receiver functions. *Tectonophysics*, *663*, 225–237. https://doi.org/10.1016/j.tecto.2015.06.028

Mancilla, F. L., Stich, D., Berrocoso, M., Martín, R., Morales, J., Fernández-Ros, et al. (2013). Delamination in the Betic Range: Deep structure, seismicity, and GPS motion. *Geology*, *41*(3), 307–310. https://doi.org/10.1130/G33733.1

Marín-Lechado, C., Galindo-Zaldívar, J., Gil, A. J., Borque, M. J., de Lacy, M. C., Pedrera, A., et al. (2010). Levelling profiles and a GPS network to monitor the active folding and faulting deformation in the Campo de Dalias (Betic Cordillera, Southeastern Spain). *Sensors*, *10*(4), 3504–3518. https://doi.org/10.3390/s100403504

Marín-Lechado, C., Galindo-Zaldívar, J., Rodríguez-Fernández, L. R., Serrano, I., & Pedrera, A. (2005). Active faults, seismicity and stresses in an internal boundary of a tectonic arc (Campo de Dalías and Níjar, southeastern Betic Cordilleras, Spain). *Tectonophysics*, *396*(1–2), 81–96. https://doi.org/10.1016/j.tecto.2004.11.001

Martínez-Martínez, J. M., Booth-Rea, G., Azañón, J. M., & Torcal, F. (2006). Active transfer fault zone linking a segmented extensional system (Betics, southern Spain): Insight into heterogeneous extension driven by edge delamination. *Tectonophysics*, *422*(1–4), 159–173. https://doi.org/10.1016/j.tecto.2006.06.001

Martínez-Martínez, J. M., Soto, J. I., & Balanyá, J. C. (2002). Orthogonal folding of extensional detachments: Structure and origin of the Sierra Nevada elongated dome (Betics, SE Spain). *Tectonics*, *21*(3), 3–1. https://doi.org/10.1029/2001TC001283

Martínez-Moreno, F. J., Galindo-Zaldívar, J., Pedrera, A., Teixidó, T., Peña, J. A., & González-Castillo, L. (2015). Regional and residual anomaly separation in microgravity maps for cave detection: The case study of Gruta de las Maravillas (SW Spain). *Journal of Applied Geophysics*, *114*, 1–11. https://doi.org/10.1016/j.jappgeo.2015.01.001

Medina-Cascales, I., Martín-Rojas, I., García-Tortosa, F. J., Peláez, J. A., & Alfaro, P. (2020). Geometry and kinematics of the Baza Fault (central Betic Cordillera, S Spain): Insights into its seismic potential. *Geológica Acta*, *18*, 1–25. https://doi.org/10.1344/GeologicaActa2020.18.11

Morales, J., Serrano, I., Jabaloy, A., Galindo-Zaldívar, J., Zhao, D., Torcal, F., et al. (1999). Active continental subduction beneath the Betic Cordillera and the Alboran Sea. *Geology*, *27*(8), 735–738. https://doi.org/10.1130/0091-7613(1999)027%3C0735:ACSBTB%3E2.3.CO;2

Morales, J., Serrano, I., Vidal, F., & Torcal, F. (1997). The depth of the earthquake activity in the Central Betics (Southern Spain). *Geophysical Research Letters*, *24*(24), 3289–3292. https://doi.org/10.1029/97GL03306

Morales, J., Vidal, F., De Miguel, F., Alguacil, G., Posadas, A. M., Ibáñez, J. M., et al. (1990). Basement structure of the Granada basin, Betic Cordilleras, southern Spain. *Tectonophysics*, *177*(4), 337–348. https://doi.org/10.1016/0040-1951(90)90394-N

Morley, C. K. (1993). Discussion of origins of hinterland basins to the Rif-Betic Cordillera and Carpathians. *Tectonophysics*, *226*(1–4), 359–376. https://doi.org/10.1016/0040-1951(93)90127-6

Nagy, D. (1966). The gravitational attraction of a right rectangular prism. *Geophysics*, *31*(2), 362–371. https://doi.org/10.1190/1.1439779

Niemi, N. A., Wernicke, B. P., Friedrich, A. M., Simons, M., Bennett, R. A., & Davis, J. L. (2004). BARGEN continuous GPS data across the eastern Basin and Range province, and implications for fault system dynamics. *Geophysical Journal International*, *159*(3), 842–862. https://doi.org/10.1111/j.1365-246X.2004.02454.x

Noda, H., & Lapusta, N. (2013). Stable creeping fault segments can become destructive as a result of dynamic weakening. *Nature*, *493*(7433), 518–521. https://doi.org/10.1038/nature11703

Papanikolaou, I. D., Roberts, G. P., & Michetti, A. M. (2005). Fault scarps and deformation rates in Lazio–Abruzzo, Central Italy: Comparison between geological fault slip-rate and GPS data. *Tectonophysics*, *408*(1–4), 147–176. https://doi.org/10.1016/j.tecto.2005.05.043

Pedley, R. C., Busby, J. P., & Dabek, Z. K. (1993). *GRAVMAG user manual–interactive 2.5 D gravity and magnetic modelling. British Geological Survey* (Technical Report WK/93/26/R). British Geological Survey.

Pedrera, A., Ruiz-Constán, A., Galindo-Zaldívar, J., Chalouan, A., Sanz de Galdeano, C., Marín-Lechado, C., et al. (2011). Is there an active subduction beneath the Gibraltar orogenic arc? Constraints from Pliocene to present-day stress field. *Journal of Geodynamics*, *52*(2), 83–96. https://doi.org/10.1016/j.jog.2010.12.003

Pérez-López, A., & Sanz de Galdeano, C. (1994). Tectónica de los materiales triásicos en el sector central de la Zona Subbética (Cordillera Bética). *Revista de la Sociedad Geologica de Espana*, *7*, 141–153. Retrieved from http://hdl.handle.net/10261/29309

Pérez-Peña, J. V., Azañón, J. M., Azor, A., Booth-Rea, G., Galve, J. P., Roldán, F. J., et al. (2015). Quaternary landscape evolution driven by slab-pull mechanisms in the Granada Basin (Central Betics). *Tectonophysics*, *663*, 5–18. https://doi.org/10.1016/j.tecto.2015.07.035

Pérez-Peña, J. V., Azañón, J. M., Azor, A., Delgado, J., & González-Lodeiro, F. (2009). Spatial analysis of stream power using GIS: SLk anomaly maps. *Earth Surface Processes and Landforms*, *34*(1), 16–25. https://doi.org/10.1002/esp.1684

Pérez-Peña, J. V., Azañón, J. M., Booth-Rea, G., Azor, A., & Delgado, J. (2009). Differentiating geology and tectonics using a spatial autocorrelation technique for the hypsometric integral. *Journal of Geophysical Research*, *114*(F2). https://doi.org/10.1029/2008JF001092

Pérouse, E., Vernant, P., Chéry, J., Reilinger, R., & McClusky, S. (2010). Active surface deformation and sub-lithospheric processes in the western Mediterranean constrained by numerical models. *Geology*, *38*(9), 823–826. https://doi.org/10.1130/G30963.1

Piccinini, D., Cattaneo, M., Chiarabba, C., Chiaraluce, L., De Martin, M., Di Bona, M., et al. (2003). A microseismic study in a low seismicity area of Italy: The Città di Castello 2000-2001 experiment. *Annals of Geophysics*, *46*(6). https://doi.org/10.4401/ag-3476

Platt, J. P., & Vissers, R. L. M. (1989). Extensional collapse of thickened continental lithosphere: A working hypothesis for the Alboran Sea and Gibraltar arc. *Geology*, *17*(6), 540–543. https://doi.org/10.1130/0091-7613(1989)017%3C0540:ECOTCL%3E2.3.CO;2

Pous, J., Queralt, P., Ledo, J. J., Roca, E., Garcia, X., & Marcuello, A. (1995). Electrical conductive structure of the central Betics from magnetotelluric data. *Revista de la Sociedad Geologica de Espana*, *8*(4), 513–517.

Proffett, Jr., J. M. (1977). Cenozoic geology of the Yerington district, Nevada, and implications for the nature and origin of Basin and Range faulting. *Geological Society of America Bulletin*, *88*(2), 247–266. https://doi.org/10.1130/0016-7606(1977)88%3C247:CGOTYD%3E2.0.CO;2

QAFI. (2021). *Quaternary faults database of Iberia*. Retrieved from https://info.igme.es/qafi/

Reinhardt, L. J., Dempster, T. J., Shroder, Jr., J. F., & Persano, C. (2007). Tectonic denudation and topographic development in the Spanish Sierra Nevada. *Tectonics*, *26*(3). https://doi.org/10.1029/2006TC001954

Reiter, F., Lenhardt, W. A., & Brandner, R. (2005). Indications for activity of the Brenner Normal Fault zone (Tyrol, Austria) from seismological and GPS data. *Australian Journal of Earth Sciences*, *97*, 16–23.

Rey, P. F., Teyssier, C., Kruckenberg, S. C., & Whitney, D. L. (2011). Viscous collision in channel explains double domes in metamorphic core complexes. *Geology*, *39*(4), 387–390. https://doi.org/10.1130/G31587.1

Rigo, A., Lyon-Caen, H., Armijo, R., Deschamps, A., Hatzfeld, D., Makropoulos, K., et al. (1996). A microseismic study in the western part of the Gulf of Corinth (Greece): Implications for large-scale normal faulting mechanisms. *Geophysical Journal International*, *126*(3), 663–688. https://doi.org/10.1111/j.1365-246X.1996.tb04697.x

Rodríguez-Fernández, J., & Sanz de Galdeano, C. (2006). Late orogenic intramontane basin development: The Granada basin, Betics (southern Spain). *Basin Research*, *18*(1), 85–102. https://doi.org/10.1111/j.1365-2117.2006.00284.x

Rosenberg, C. L., & García, S. (2011). Estimating displacement along the Brenner Fault and orogen-parallel extension in the Eastern Alps. *International Journal of Earth Sciences*, *100*(5), 1129–1145. https://doi.org/10.1007/s00531-011-0645-3

Ruano, P., Galindo-Zaldívar, J., & Jabaloy, A. (2004). Recent tectonic structures in a transect of the Central Betic Cordillera. *Pure and Applied Geophysics*, *161*(3), 541–563. https://doi.org/10.1007/s00024-003-2462-5

Ruiz, A. M., Ferhat, G., Alfaro, P., Sanz de Galdeano, C., de Lacy, M. C., et al. (2003). Geodetic measurements of crustal deformation on NW–SE faults of the Betic Cordillera, southern Spain, 1999–2001. *Journal of Geodynamics*, *35*(3), 259–272. https://doi.org/10.1016/S0264-3707(02)00134-5

Ruiz-Bustos, A. (2002). Características climáticas y estratigráficas de los sedimentos continentales de la Cordillera Bética durante el Plioceno, a partir de las faunas de mamíferos. *Pliocenica*, *2*, 44–64.

Ruiz-Constán, A., Galindo-Zaldívar, J., Pedrera, A., Celerier, B., & Marín-Lechado, C. (2011). Stress distribution at the transition from subduction to continental collision (northwestern and central Betic Cordillera). *Geochemistry, Geophysics, Geosystems*, *12*(12). https://doi.org/10.1029/2011GC003824

Ruiz-Constán, A., Pedrera, A., Galindo-Zaldívar, J., Pous, J., Arzate, J., Roldn-García, F. J., et al. (2012). Constraints on the frontal crustal structure of a continental collision from an integrated geophysical research: The central-western Betic Cordillera (SW Spain). *Geochemistry, Geophysics, Geosystems*, *13*(8). https://doi.org/10.1029/2012GC004153

Ruiz-Constán, A., Stich, D., Galindo-Zaldívar, J., & Morales, J. (2009). Is the northwestern Betic Cordillera mountain front active in the context of the convergent Eurasia–Africa plate boundary? *Terra Nova*, *21*(5), 352–359. https://doi.org/10.1111/j.1365-3121.2009.00886.x

Santos-Bueno, N., Fernández-García, C., Stich, D., Mancilla, F. d. L., Martín, R., Molina-Aguilera, A., & Morales, J. (2019). Focal mechanisms for subcrustal earthquakes beneath the Gibraltar Arc. *Geophysical Research Letters*, *46*, 2534–2543. https://doi.org/10.1029/2018GL081587

Sanz de Galdeano, C. S. (1990). Geologic evolution of the Betic Cordilleras in the Western Mediterranean, Miocene to the present. *Tectonophysics*, *172*(1–2), 107–119. https://doi.org/10.1016/0040-1951(90)90062-D

Sanz de Galdeano, C. S., & Alfaro, P. (2004). Tectonic significance of the present relief of the Betic Cordillera. *Geomorphology*, *63*(3–4), 175–190. https://doi.org/10.1016/j.geomorph.2004.04.002

Sanz de Galdeano, C. S., Andreo, B., Garcıa-Tortosa, F. J., & López-Garrido, A. C. (2001). The Triassic palaeogeographic transition between the Alpujarride and Malaguide complexes. Betic–Rif Internal Zone (S Spain, N Morocco). *Palaeogeography, Palaeoclimatology, Palaeoecology*, *167*(1–2), 157–173. https://doi.org/10.1016/S0031-0182(00)00236-4

Sanz de Galdeano, C. S., Peláez, J. A., & López-Casado, C. (2003). Seismic potential of the main active faults in the Granada Basin (southern Spain). *Pure and Applied Geophysics*, *160*(8), 1537–1556. https://doi.org/10.1007/s00024-003-2359-3

Sanz de Galdeano, C. S., Shanov, S., Galindo-Zaldívar, J., Radulov, A., & Nikolov, G. (2010). A new tectonic discontinuity in the Betic Cordillera deduced from active tectonics and seismicity in the Tabernas Basin. *Journal of Geodynamics*, *50*(2), 57–66. https://doi.org/10.1016/j.jog.2010.02.005

Sanz de Galdeano, C. S., Tortosa, G. F. J., Peláez, J. A., Alfaro García, P., Azañón, J. M., et al. (2012). Main active faults in the Granada and Guadix-Baza basins (Betic Cordillera). *Journal of Iberian Geology*, *38*, 209–223. https://doi.org/10.5209/rev_jige.2012.v38.n1.39215

Searle, M. P., & Lamont, T. N. (2020). Compressional metamorphic core complexes, low-angle normal faults and extensional fabrics in compressional tectonic settings. *Geological Magazine*, *157*(1), 101–118. https://doi.org/10.1017/S0016756819000207

Seber, D., Barazangi, M., Ibenbrahim, A., & Demnati, A. (1996). Geophysical evidence for lithospheric delamination beneath the Alboran Sea and Rif–Betic mountains. *Nature*, *379*(6568), 785. https://doi.org/10.1038/379785a0

Selverstone, J. (1988). Evidence for east–west crustal extension in the Eastern Alps: Implications for the unroofing history of the Tauern Window. *Tectonics*, *7*, 87–105. https://doi.org/10.1029/TC007i001p00087

Serrano, I. (1999). *Distribución espacial de la sismicidad en las Cordilleras Béticas-Mar de Alborán* (Doctoral dissertation). University of Granada.

Serrano, I., Morales, J., Vidal, F., & Torcal, F. (1996). Mecanismos focales en la cuenca de Granada. In F. Vidal, & M. Espinar (Eds.), *Libro Homenaje a Fernando de Miguel Martinez* (pp. 619–640). Universidad de Granada.

Serrano, I., Zhao, D., & Morales, J. (2002). 3-D crustal structure of the extensional Granada Basin in the convergent boundary between the Eurasian and African plates. *Tectonophysics*, *344*(1–2), 61–79. https://doi.org/10.1016/S0040-1951(01)00201-3

Sibson, R. H. (1985). A note on fault reactivation. *Journal of Structural Geology*, *7*(6), 751–754. https://doi.org/10.1016/0191-8141(85)90150-6

SIGEOF. (2021). *Geophysical information system*. INFOIGME. Retrieved from http://info.igme.es/SIGEOF/

Silva, P. G., Goy, J. L., Somoza, L., Zazo, C., & Bardají, T. (1993). Landscape response to strike-slip faulting linked to collisional settings: Quaternary tectonics and basin formation in the Eastern Betics, southeastern Spain. *Tectonophysics*, *224*(4), 289–303. https://doi.org/10.1016/0040-1951(93)90034-H

SIS. (2021). *Earthquake catalogue*. IGN. Retrieved from https://www.ign.es/web/ign/portal/sis-catalogo-terremotos/

SMT. (2021). *Seismic moment tensor*. IGN. Retrieved from https://www.ign.es/web/ign/portal/tensor-momento-sismico/

Spakman, W., Chertova, M. V., van den Berg, A., & van Hinsbergen, D. J. (2018). Puzzling features of western Mediterranean tectonics explained by slab dragging. *Nature Geoscience*, *11*(3), 211. https://doi.org/10.1038/s41561-018-0066-z

Sparacino, F., Palano, M., Peláez, J. A., & Fernández, J. (2020). Geodetic deformation versus seismic crustal moment-rates: Insights from the Ibero-Maghrebian region. *Remote Sensing*, *12*, 952. https://doi.org/10.3390/rs12060952

Stewart, I. S., & Hancock, P. L. (1991). Scales of structural heterogeneity within neotectonic normal fault zones in the Aegean region. *Journal of Structural Geology*, *13*(2), 191–204. https://doi.org/10.1016/0191-8141(91)90066-R

Stich, D., Ammon, C. J., & Morales, J. (2003). Moment tensor solutions for small and moderate earthquakes in the Ibero-Maghreb region. *Journal of Geophysical Research*, *108*, 2148. https://doi.org/10.1029/2002JB002057

Stich, D., Martín, R., & Morales, J. (2010). Moment tensor inversion for Iberia-Maghreb earthquakes 2005-2008. *Tectonophysics*, *483*, 390–398. https://doi.org/10.1016/j.tecto.2009.11.006

Stich, D., Serpelloni, E., Mancilla, F. L., & Morales, J. (2006). Kinematics of the Iberia-Maghreb plate contact from seismic moment tensors and GPS observations. *Tectonophysics*, *426*, 295–317. https://doi.org/10.1016/j.tecto.2006.08.004

Telford, W. M., Geldart, L. P., & Sheriff, R. E. (1990). *Applied geophysics* (p. 1). Cambridge University Press.

Thiebot, E., & Gutscher, M. A. (2006). The Gibraltar Arc seismogenic zone (part 1): Constraints on a shallow east dipping fault plane source for the 1755 Lisbon earthquake provided by seismic data, gravity and thermal modeling. *Tectonophysics*, *426*(1–2), 135–152. https://doi.org/10.1016/j.tecto.2006.02.024

Torres-Roldán, R. L., Poli, G., & Peccerillo, A. (1986). An Early Miocene arc-tholeiitic magmatic dike event from the Alboran Sea—Evidence for precollisional subduction and back-arc crustal extension in the westernmost Mediterranean. *Geologische Rundschau*, *75*(1), 219–234. https://doi.org/10.1007/BF01770190

Tucker, G. E., McCoy, S. W., Whittaker, A. C., Roberts, G. P., Lancaster, S. T., & Phillips, R. (2011). Geomorphic significance of postglacial bedrock scarps on normal-fault footwalls. *Journal of Geophysical Research*, *116*(F1). https://doi.org/10.1029/2010JF001861

Vidal, F. (1986). *Sismotectónica de la región Béticas-Mar de Alboran* (Doctoral dissertation). University of Granada.

Vissers, R. L. M., Platt, J. P., & Van der Wal, D. (1995). Late orogenic extension of the Betic Cordillera and the Alboran Domain: A lithospheric view. *Tectonics*, *14*, 786–803. https://doi.org/10.1029/95TC00086

Wernicke, B. (1981). Low-angle normal faults in the Basin and Range Province: Nappe tectonics in an extending orogen. *Nature*, *291*(5817), 645–648. https://doi.org/10.1038/291645a0

Wernicke, B. (1995). Low-angle normal faults and seismicity: A review. *Journal of Geophysical Research*, *100*(B10), 20159–20174. https://doi.org/10.1029/95JB01911

Wernicke, B., & Axen, G. J. (1988). On the role of isostasy in the evolution of normal fault systems. *Geology*, *16*(9), 848–851. https://doi.org/10.1130/0091-7613(1988)016%3C0848:OTROII%3E2.3.CO;2

Wortel, M. J. R., & Spakman, W. (1992). Structure and dynamics of subducted lithosphere in the Mediterranean region. *Proceedings of the Koninklijke Nederlandse Akademie van Wetenschappen*, *95*(3), 325–347.

Wortel, M. J. R., & Spakman, W. (2000). Subduction and slab detachment in the Mediterranean-Carpathian region. *Science*, *290*(5498), 1910–1917. https://doi.org/10.1126/science.290.5498.1910

Zeck, H. P. (1996). Betic-Rif orogeny: Subduction of Mesozoic Tethys lithosphere under eastward drifting Iberia, slab detachment shortly before 22 Ma, and subsequent uplift and extensional tectonics. *Tectonophysics*, *254*(1–2), 1–16. https://doi.org/10.1016/0040-1951(95)00206-5

Zeck, H. P., Monié, P., Villa, I. M., & Hansen, B. T. (1992). Very high rates of cooling and uplift in the Alpine belt of the Betic Cordilleras, southern Spain. *Geology*, *20*(1), 79–82. https://doi.org/10.1130/0091-7613(1992)020%3C0079:VHROCA%3E2.3.CO;2